Modelling the impact of wood density dependent tree mortality on the spatial distribution of Amazonian vegetation carbon

Mathilda Hancock[1], Stephen Sitch[1], Fabian J. Fischer[2], Jérôme Chave[2], Michael O'Sullivan[3], Dominic Fawcett[1], and Lina M. Mercado[1,4]

[1]College of Life and Environmental Sciences, University of Exeter, EX4 4RJ, Exeter, UK
[2]Laboratoire Évolution et Diversité Biologique (UMR5174) Bâtiment 4R1, 118 route de Narbonne, 31062 CEDEX 9, Toulouse, France
[3]College of Engineering, Mathematics and Physical Sciences, University of Exeter, EX4 4QF, Exeter, UK
[4]UK Centre for Ecology and Hydrology, Benson Lane, Wallingford, OX10 8BB, UK
Correspondence: Mathilda Hancock (mathilda.hancock@outlook.com)

Abstract. Spatially heterogeneous plant mortality rates are an important predictor of the distribution of vegetation carbon in Amazonia. Reproducing the spatial gradients of vegetation carbon in Amazonia and the observed decline in the intact Amazonian carbon sink since 1990 is a challenge faced by dynamic global vegetation models (DGVMs). In this paper, we implement spatially variable mortality rates in TRIFFID, the DGVM currently coupled to the Joint UK Land Environment Simulator (JULES), and compare with the standard model which assumes a homogeneous mortality rate. Spatially variable gridded fields

5 of Amazonian tree mortality are created using a well-known relationship between mortality and wood density, and three independent wood density maps. The diversified mortality scheme substantially improves the representation of vegetation carbon in TRIFFID when compared to observations, with a 90% reduction in model bias and an increase in the Pearson correlation coefficient with observed biomass. JULES now captures the observed variability of both mortality and vegetation carbon to

10 a greater extent, demonstrating the potential of using easily-measured traits, like wood density, to add spatial and functional diversity into DGVMs. Despite this, the spatial variation of vegetation carbon simulated with the new mortality fields (with standard deviation 15 MgCha^{-1}) is still less than half of the variation in the observed data (standard deviation 35 MgCha^{-1}). Future work should consider the effects of additional processes, like fire, drought and the phosphorus cycle, on the simulated distribution of vegetation carbon in the Amazon.

15 *Copyright statement.* TEXT

1 Introduction

The Amazon forest is hugely important for regional and global carbon cycles (Brienen et al., 2015; Avitabile et al., 2016; Steffen et al., 2018), biodiversity (Myers et al., 2000; Ter Steege et al., 2016) and hydrological cycles (Zemp et al., 2014; Badger and Dirmeyer, 2016). This diverse ecosystem is estimated to contain between 6700 and 16000 tree species (Ter Steege

20 et al., 2013, 2016; Cardoso et al., 2017), most of which are extremely rare (Ter Steege et al., 2013). As well as taxonomic diversity, there is great spatial diversity in the environmental properties affecting the Amazon forest (including soil characteristics (Quesada et al., 2010), climate (Malhi and Wright, 2004) and anthropogenic disturbance (Bullock et al., 2020)). In conjunction with this environmental heterogeneity and with changes in species composition comes a high diversity of plant functional traits (Chave et al., 2009; Fyllas et al., 2009). Such variations are strong predictors of the distribution of above

25 ground biomass (AGB) in Amazonia (Baker et al., 2004; Malhi et al., 2015; Johnson et al., 2016). Estimates from forest plots and remote sensing suggest that Amazonia stores almost half of the above ground carbon in global tropical forests (Malhi et al., 2006; Saatchi et al., 2007; Avitabile et al., 2016). Between 1990 and 2007, intact Amazonian forests acted as a net carbon sink (Brienen et al., 2015), but the size of this large intact sink is declining (Brienen et al., 2015; Hubau et al., 2020), and regions of the wider Amazon forest (including disturbed forests) could already act as a source (Gatti et al., 2021; Harris et al., 2021).

30 There is a general spatial trend in the diverse plant strategies across Amazonia. More dynamic forests with fertile soils are found in the south-west, selecting for fast growing species with high mortality rates (Quesada et al., 2012). Here, AGB is lower and more heterogeneous (Mitchard et al., 2014; Rödig et al., 2017). In the northern and eastern Amazon, soil is less fertile and its physical properties improve (meaning deeper, non-waterlogged soils with shallow slopes) (Quesada et al., 2010), selecting for slow growing and low mortality species (Quesada et al., 2012). These forests have high AGB (Malhi et al., 2006; Mitchard

35 et al., 2014; Avitabile et al., 2016). Meanwhile, the fringes of the Amazon forest and the south-east have high mortality rates and lower AGB due to the interlinking effects of anthropogenic disturbance and climate anomalies (Bullock et al., 2020; Esquivel-Muelbert et al., 2020). The mean mortality rate varies between these regions by up to a factor of two (Esquivel-Muelbert et al., 2020).

Wood density is an important plant trait linking the above trends in mortality and AGB across Amazonia. Forest communities

40 in the south-west tend to contain species with lower wood density, and community averaged wood density increases towards the north-east (Baker et al., 2004; Chave et al., 2006; Mitchard et al., 2014). Wood density variation accounts for 45% or 30% of AGB variation (depending on the model of biomass used) (Baker et al., 2004). Additionally, studies across the Neotropics have found a negative relationship between wood density and both mortality (Muller-Landau, 2004; Nascimento et al., 2005; Poorter et al., 2008; Wright et al., 2010; Kraft et al., 2010; Greenwood et al., 2017; Esquivel-Muelbert et al., 2020) and growth

45 rates (Nascimento et al., 2005; Poorter et al., 2008; Wright et al., 2010; Francis et al., 2017). This is the basis for the wood economics spectrum; species at the "conservative" end are slow growing, have low mortality rates and allocate carbon to create dense wood, with thicker non-conducting fibre walls (Chave et al., 2009), and narrower, more densely packed vessels (McCulloh et al., 2011). At the other extreme, fast growing "acquisitive" species have higher mortality rates and less dense wood.

50 There are many ways in which higher wood density could offer an advantageous resource-use strategy. The first advantage is mechanical strength, as higher wood density is strongly correlated with wood elasticity to bending and rupture in laboratory (Chave et al., 2009) and field measurements (Van Gelder et al., 2006). Secondly, higher wood density may confer resistance to drought induced mortality (Greenwood et al., 2017) by increasing hydraulic safety (Fu and Meinzer, 2019). In a study of 59 species, Liang et al. (2021) found that lethal water potential becomes more negative with increasing wood density. High density

55 wood could instead be advantageous because it enables trunks to have lower surface area for the same mechanical strength, possibly leading to lower rates of maintenance respiration (Larjavaara and Muller-Landau, 2010). For acquisitive species with shorter lifespans, the long term benefit of low maintenance cost is smaller than the short-term benefit of low wood construction cost (i.e. low wood density). Trunk respiration is poorly understood and more data are needed to support this hypothesis.

Given the evidence above, modelling mortality rates in the Amazon as spatially constant is not only unrealistic, but has
60 implications for AGB predictions (Delbart et al., 2010; Galbraith et al., 2013; Castanho et al., 2013; Rödig et al., 2017). In fact, multiple studies (Malhi et al., 2015; Johnson et al., 2016; Magnabosco Marra et al., 2018) highlight that mortality rates are an important predictor of spatial variation in AGB across Amazonia. For example, data from long term forest plots show that variation in mortality rates explains the lower biomass of seasonally dry tropical forests compared to humid forests (Malhi et al., 2015). Johnson et al. (2016) use an expanded range of plots to show that stem mortality rates are the most
65 important predictor of AGB across the whole Amazon region, over woody net primary productivity (NPP). Dynamic global vegetation models (DGVMs) which use plant functional types (PFTs), like the DGVM used in this paper, often use spatially and temporally constant mortality rates or woody residence times for each PFT, though some include processes like negative carbon balance, aging and fire in their mortality models (Galbraith et al., 2013; Pugh et al., 2020). Previous studies (Delbart et al., 2010; Castanho et al., 2013) have acknowledged the importance of adding spatially varying aspects of forest function
70 into DGVMs, and have demonstrated that this improves the simulated biomass distribution in Amazonia. Castanho et al. (2013) introduced a spatially variable woody residence time, among other parameters, into the Integrated Biosphere Simulator (IBIS). The addition of spatially varying parameters improved the correlation of the simulated output with observed woody biomass hugely (R=0.52) compared to a simulation with homogeneous parameters (R=-0.006). Delbart et al. (2010) found that the DGVM ORCHIDEE could better reproduce observed patterns of woody AGB when mortality rates were calculated using a
75 prescribed relationship with woody NPP. This relationship was back-calculated from observations of woody NPP and carbon residence time. This showed, as a proof-of-concept, that correctly formulating mortality can improve AGB estimation, but it would not be easy to extrapolate this approach to another DGVM without prescribing data in a similar way.

This paper focuses on the Joint UK Land Environment Simulator (JULES) (Best et al., 2011; Clark et al., 2011), which is coupled to the TRIFFID DGVM (Top-down Representation of Interactive Foliage and Flora Including Dynamics) (Cox,
80 2001). JULES, within the UK Earth System Model, is included in the Coupled Model Intercomparison Project and the Inter-governmental Panel on Climate Change assessment reports (Zelinka et al., 2020) and strengthens estimations of present day annual global carbon budgets (Friedlingstein et al., 2020). Carbon dynamics in JULES have previously been evaluated against observed AGB, showing that JULES underestimates the spatial variation of AGB in Amazonia (Johnson et al., 2016). This may be because spatially constant background mortality rates are prescribed to each PFT. In this work, we explore the impact of a
85 spatially varying mortality rate on the distribution of Amazonian vegetation carbon simulated by JULES. In the absence of a high resolution map of mortality rates across the Amazon forest, the relationship between species wood density and mortality rate is exploited to generate input maps of mortality for JULES across Amazonia, which better reflect the 2-fold variation in mean mortality rates between different Amazonian regions (Esquivel-Muelbert et al., 2020). Simulated AGB is evaluated against observations of vegetation carbon based on remote sensing and forest inventories. The key questions addressed in this

90 paper are: *(1)* Does adding a spatially varying, wood density dependent mortality rate improve the simulated spatial distribution of vegetation carbon? *(2)* Are other processes, apart from those implicit in the wood density – mortality relationship, needed to correctly model mortality heterogeneity across Amazonia? *(3)* Can variation in mortality alone fully describe observed spatial variability in above ground carbon stocks?

2 Methods

95 ### 2.1 JULES model outline and new mortality scheme

JULES is a land surface scheme incorporating carbon fluxes, hydrology, vegetation dynamics and plant physiology (Best et al., 2011; Clark et al., 2011). In each land surface grid cell, the carbon fluxes for different PFTs are calculated mechanistically by models of plant photosynthesis and respiration. The vegetation dynamics are then updated in TRIFFID (Cox, 2001), which determines the net carbon available for growth and coverage spreading of each PFT, competition between PFTs and the result-

100 ing change in the fractional area coverage of each PFT. Carbon lost from the vegetation pool, through large-scale disturbance and litterfall, enters a soil model which calculates microbial respiration. Once the vegetation coverage and carbon have been updated in TRIFFID, land surface properties are recalculated, allowing feedbacks when coupled to an earth system model.

Mortality is included in TRIFFID via the change in fractional coverage (ν) with time for a given PFT, in Eq. (1):

$$C_{veg}\frac{d\nu}{dt} = \lambda\Pi\nu\left(1 - \sum_{j}c_{ij}\nu_{j}\right) - \gamma\nu C_{veg}, \tag{1}$$

105 where Π is the net primary productivity of the PFT of interest and λ is the spreading fraction, the proportion of carbon used for increasing its coverage. The competition coefficients, c_{ij}, determine the extent to which increased coverage of other PFTs affects the PFT in question and are calculated as a function of PFT height (Harper et al., 2018). The important term in the context of this study is the mortality rate, γ, which, for each PFT, determines the rate at which vegetation coverage is lost through background mortality processes. It is usually set to a constant value for each PFT; for example in JULES version 5.4

110 this value is 0.007 yr^{-1} for the tropical broadleaf evergreen tree (BET-Tr) PFT. In order to allow γ to vary with location, here it was prescribed as an extra ancillary variable with a unique value at every simulated land point. The input mortality datasets were derived from wood density data for Amazonia using relationships found in literature (see Sect. 2.2). It was only through the variable γ in Eq. (1) that wood density could influence the vegetation carbon simulated by JULES.

The BET-Tr PFT is the dominant type in the Amazon (Harper et al., 2016, 2018), therefore, for the purpose of this study

115 only the mortality rate of this PFT was allowed to vary. To isolate the effects of introducing variable mortality into the dominant Amazonian PFT from other effects, we removed competition from the remaining 12 PFTs (8 natural and 4 agricultural, described in (Harper et al., 2016, 2018)) by setting their mortality rates to very noncompetitive values.

2.2 Wood density – mortality equations

Four equations describing the wood density – mortality relationship from literature applicable to tropical forests were tested in
120   this study (Table 1). They were selected because they are based on data collected in Amazonia or have been previously used
for modelling in Amazonia. Wood density refers to the *wood specific gravity*, the ratio of the mass of wood with 0% moisture
content to its volume when water-saturated, in grams per centimetre cubed.

Table 1. The wood density – mortality models included in this study. The control mortality rate is the value originally used in JULES (Harper
et al., 2018). ρ_{max} is the maximum wood density. Mortality (γ) is in units per year.

Mortality Model	Equation	Reference
M1	$\gamma = 0.014 + 0.150 \left(1 - \frac{\rho}{\rho_{max}}\right)$	(Moorcroft et al., 2001)
M2	$\gamma = 0.029 - 0.022\rho$	(Kraft et al., 2010)
M3	$\gamma = 10^{-2.66 + \frac{0.255}{\rho}}$	(King et al., 2006; Sakschewski et al., 2015)
M4	$\gamma = 0.025 \left(1 - \frac{\rho}{\rho_{max}}\right)$	(Maréchaux and Chave, 2017)
Control	$\gamma = 0.007$	(Harper et al., 2018)

In M1 and M4, the wood density term is normalised by a maximum wood density, ρ_{max}. The maximum wood density
attainable under the conditions of lignin and cellulose packing is around 1.5 gcm^{-3} (Siau, 1984; Chave et al., 2009), but a
125   more realistic value for maximum species wood density is 1.25 gcm^{-3}, given that only 0.02% of species in the Global Wood
Density Database have wood density greater than this value (Zanne et al., 2009). For the purposes of our large scale application,
this value was chosen to ensure no grid cell was assigned a negative mortality rate. The disadvantage of this method is that
the gradients of the two equations are effectively changed when ρ_{max} is altered from the values presented in the original
papers (formerly in M1, ρ_{max} = 0.9 gcm^{-3} and in M4, ρ_{max} = 1.0 gcm^{-3}). Despite this, the equations were included in the
130   experiment as extremes (M1 has a very large gradient and intercept compared to the others, whereas M4 has the lowest gradient
and intercept) to explore the model sensitivity. The four equations used and the original versions of M1 and M4 are visualised
in Fig. A1.

It is important for regional-scale modelling that the equations used are based on taxonomically and spatially diverse data
from suitable locations. M1 was not derived from a directly measured correlation between wood density and mortality, but was
135   fitted to give reasonable mortality rates for early and late successional plant types. The mortality rates for early successional
types were based on observations from a five year period after cutting and burning on one site in Venezuela (Uhl and Jordan,
1984). The late successional mortality was based on several sites across tropical South America (Swaine et al., 1987; Lugo and
Scatena, 1996). M1 was the only equation using data from disturbed forests. M2 was derived directly by fitting the relationship
between mortality and wood density (R^2=0.39); an improvement on M1. The data are from only one site (Yasuní, Ecuador), but

140   include 364 species (1–41,013 individuals per species) (Kraft et al., 2010). Wood density values for each species were taken from the Global Wood Density Database database (Zanne et al., 2009). M3 was obtained from a logarithmic fit (R^2=0.62) of mortality against wood density measurements taken from 21 species (1–4 individuals per species) from two forest sites in Malaysia (King et al., 2006). The fact that the study sites did not match the location of this analysis is obviously a disadvantage; however this equation is included in the mortality model used by Sakschewski et al. (2015) in LPJmL-FIT, specifically for

145   Amazonia. This equation merits inclusion here because it affords the opportunity to test whether a non-linear relationship can better reproduce biomass variation. Finally, in M4, the gradient parameter was tuned in the original publication (Maréchaux and Chave, 2017) so that AGB, NPP, leaf area index and stem density outputs best reproduced observational data from two plots in French Guiana; this equation is not based on direct observations of mortality data.

The strength of the relationship between wood density and mortality differs geographically but, reportedly, this may be due

150   to differences in sample size between the plots measured (Kraft et al., 2010). The slope of M2 is within the 95% confidence range of the coefficients for the two other Neotropical rainforest sites used in the same investigation (La Planada, Colombia, and Barro Colorado Island, Panama), although the intercept is not. This offers some reassurance that the strength of the wood density – mortality relationship is relatively stable over the simulated area. All equations were assumed to apply over Amazonia in this study for simplicity and for want of comprehensive data on the strength of the relationship across the whole region.

155   ## 2.3   Wood density data and regridding

Three maps of wood density for the Amazon forest were used in this study. The derivation method impacted the range of wood density values present in the maps, so the three datasets provided another means of testing the sensitivity of JULES outputs.

The first map of wood density was created by calculating the unweighted mean wood density for all species occurring in each grid cell. Mean species values of wood density were taken from an update to the Global Wood Density Database (Zanne

160   et al., 2009). Species occurrence was predicted using species distribution models (SDMs) developed from occurrence records from the Global Biodiversity Information Facility (GBIF) (GBIF.org, 2021) and climatic layers. Henceforth this is called the "SDM-based" map. The fact that mean wood density for each grid cell is not weighted by species abundance contributes to the relatively low variation between cells, as extreme values are averaged out. This method was chosen because species abundance data with wide coverage is difficult to source for Amazonia. Similar results were achieved in a map which only included the

165   hyperdominant Amazonian species (Ter Steege et al., 2013), suggesting that weighting by abundance may not increase the wood density variation dramatically.

To create the second map, global climate covariates (TerraClimate (Abatzoglou et al., 2018)), disturbance layers and a subset of wood density pixels were used to train a regularised random forest (RF) model to predict wood density over the region, utilising the "ranger" R package. Wood density for each 25 km pixel was calculated as the unweighted average value

170   for all species with measured occurrence in the pixel, with occurrence data from the GBIF (GBIF.org, 2021). Only pixels where occurring species were well-sampled were used to train the model. A spatial autocorrelation term was added and the map was validated using buffered leave-one-out cross validation (Ploton et al., 2020). This will be referred to as the "RF-based" map of

wood density. This and the previous map did not explicitly exclude species occurrence data from human modified forests, but these forests are likely underrepresented in species collections.

175   The two maps above were regridded to match the resolution of the other ancillary data used in the modelling, $1.875°$ longitude by $1.25°$ latitude. This was achieved with area weighted regridding, where the value of each new grid cell is the mean of the overlapping source cells, weighted by their area of intersection with the new cell. New cells were masked when over 50% of the overlapping source cells were blank due to missing data; this threshold best represented the forest extent in the original maps.

180   The final wood density map was derived by spatial interpolation (kriging) of the mean wood density from 414 *intact* forest plots, using plot data from another study (Mitchard et al., 2014). This map will be referred to as the kriged map. Mitchard et al. (2014) recorded mean wood density values weighted by species basal area, primarily from RAINFOR (Peacock et al., 2007) and ATDN (Ter Steege et al., 2013) data, with species wood density values from the Global Wood Density Database (Zanne et al., 2009). Notably, there are no data from disturbed forests. These observations were interpolated across the study

185   area by ordinary kriging with a spherical variogram model ("PyKrige" package in Python). It was validated using 5-fold cross validation with a coefficient of determination, R^2=0.35.

2.4   JULES simulations over the Amazon forest

JULES was run over all Amazonian grid cells. Maps of mortality across Amazonia were generated by applying each of the four equations in Table 1 to each of three observational wood density datasets (Sect. 2.3). This resulted in 12 different mortality

190   configurations, which were fed into JULES as ancillary data in 12 separate simulations. The results were compared against a control simulation, where mortality was spatially constant with the value for the BET-Tr PFT used in the original configuration of JULES.

In this work, the earth system configuration of JULES, JULES-ES was used (Sellar et al., 2019). This is the configuration used in the TRENDY version 8 ensemble, a group of models used to simulate net biome production under standard protocols

195   for annual Global Carbon Budget assessments (Friedlingstein et al., 2020). Specifically, the TRENDY S2 experiment was used (Sitch et al., 2015), where land use is kept at pre-industrial levels throughout the simulation period. However, a shorter main run length was used, from 1900 to 2017, with 5 spin-up cycles from 1880 to 1900. The model was driven by meteorological CRU-JRA55 forcing. The spatial resolution was $1.875°$ longitude by $1.25°$ latitude and an hourly timestep was used.

2.5   Model evaluation

200   A map of vegetation carbon created by Avitabile et al. (2016), based on remote sensing and field data, was used to test the success of adding spatially variable mortality rates into JULES and is henceforth called the Avitabile map. It is a fusion of two pantropical biomass maps (Saatchi et al., 2011; Baccini et al., 2012), which were derived from Geoscience Laser Altimeter System LiDAR remote sensing data, and calibrated with field observations. The maps are fused using bias removal and weighted linear averaging in a model that was calibrated against an extensive reference dataset. The model parameters

were calibrated independently for several regions where the error patterns were deemed homogeneous in the original maps. It has 1 km resolution and combines data from 2000-2013, implicitly including disturbed and secondary forests in Amazonia.

An analysis comparing results to an alternative map of Amazonian biomass is included in Appendix B. The ESA CCI Biomass product for 2017 (Santoro and Cartus, 2021) was created using allometric relationships between AGB, canopy height and synthetic aperture radar (SAR) backscatter. L-band SAR data from ALOS-2 PALSAR-2 was merged with C-band SAR data from Sentinel-1 to reduce error, but in Amazonia the L-band data dominated almost completely. The resulting map has 100 m resolution.

AGB was converted into vegetation carbon using a conversion factor of 0.5 (Chave et al., 2005). The maps were then regridded following the method in Sect. 2.3. The regridded Avitabile and ESA CCI maps are shown in Fig. B1.

Model evaluation was also completed for *intact forests*, defined as grid cells containing forests with less than 20% disturbance. Maps of disturbed forest fraction for 2017 were calculated from degraded forest (JRC (Vancutsem et al., 2021)), secondary forest (MapBiomas Amazonia C2 (MapBiomas, 2021)) and total forest extent (MapBiomas) data. They were regridded using the method outlined in Sect. 2.3. The raw data and masked forest extent are shown in Fig. C1.

An additional experiment was conducted to test whether the observed vegetation carbon could be captured by any range of wood density. A linear regression was applied to the simulated vegetation carbon and the mortality rates of the corresponding grid cells produced from M2–4. M1 was excluded because it led to vegetation dieback. The linear fit coefficients were used to back-calculate the mortality rates needed to produce the vegetation carbon in the Avitabile map, under the assumption that mortality is its sole predictor. Then, the wood density distributions required to recreate the Avitabile map from each of M2–4 were back-calculated and compared to observed wood densities from Amazonia.

2.6 Statistical comparison

A measure of the "additional spatial variation" (ϕ) was used to show any spatial variation in the simulated vegetation carbon on top of the variation that already exists in the control simulation. Below, C_{veg} denotes vegetation carbon density and depends on the grid cell location (x). Simulated vegetation carbon density is distinguished by a hat on the variable ($\hat{C}_{veg}$), whereas the observed quantity has no hat. A bar (e.g. $\bar{\hat{C}}_{veg}$) represents the mean over all locations. If, for example, $\hat{C}_{veg}$ is the output from the M2 and RF-based wood density combination, and $\hat{C}_{veg,c}$ is the output from the control simulation:

$$\phi = (\hat{C}_{veg} - \bar{\hat{C}}_{veg}) - (\hat{C}_{veg,c} - \bar{\hat{C}}_{veg,c}). \tag{2}$$

The equations below were used to test the degree of correspondence between the simulated ($\hat{C}_{veg}(x)$) and observed ($C_{veg}(x)$) distributions of vegetation carbon. The absolute bias is defined as:

$$Bias(\hat{C}_{veg}, C_{veg}) = |\bar{\hat{C}}_{veg} - \bar{C}_{veg}|. \tag{3}$$

$$CRMSD = \sqrt{\frac{\sum_x^N \left[(\hat{C}_{veg,x} - \bar{\hat{C}}_{veg}) - (C_{veg,x} - \bar{C}_{veg})\right]^2}{N}} \tag{4}$$

In the definition for the centred root mean squared deviation (CRMSD) above, the sum is over each grid cell and N is the total number of grid cells.

$$R = \frac{\sum_x^N (\hat{C}_{veg,x} - \bar{\hat{C}}_{veg})(C_{veg,x} - \bar{C}_{veg})}{N \hat{\sigma} \sigma} \tag{5}$$

The Pearson correlation coefficient (R), defined above, uses $\hat{\sigma}$ and σ, the standard deviations of the simulated and observed
240 data, respectively.

3 Results

3.1 Wood density and mortality maps for the Amazon forest

The original SDM-based wood density map (Fig. 1a) agrees well with the RF-based map (Fig. 1b), with R^2 close to 0.9. The range of wood density values in the RF-based map was 60% larger than the range of the SDM-based map. The regridded
245 versions of these maps are shown in Fig. 1d and Fig. 1e, respectively. The kriged map is shown in Fig. 1f, with the original plot data in Fig. 1c. Although it is less accurate, this map provides an even larger range of wood density values, since the basal area weighting of the species means prevented the less abundant species (e.g. pioneer species with low wood density) from skewing averages. This results in a map with a range three times larger than that of the regridded SDM-based map, and a higher mean wood density (0.635 ± 0.048 (SD) gcm^{-3} compared to 0.580 ± 0.013 gcm^{-3} for the SDM-based map and 0.589 ± 0.017
250 gcm^{-3} for the RF-based map), perhaps reflecting the reduced importance of the pioneer species in the average.

The four wood density – mortality equations produce similar spatial distributions of mortality rates (Fig. 2) with shifted absolute values. M3 produces a mean mortality rate of ~ 0.006 yr^{-1}, similar to the homogeneous value of 0.007 yr^{-1} used in the control simulations, and low spatial variability (Figs. 2c,g,k). The other equations result in higher mean mortality rates than the homogeneous control rate. In all cases, mortality calculated from the kriged wood density data (Figs. 2i–l) has the largest
255 range and standard deviation (Table 2) and the SDM-based wood density map results in the least variation, as expected.

3.2 Simulated vegetation carbon with spatially variable mortality rate fields

The control JULES simulation shows low spatial variation in vegetation carbon (Fig. 3a), with the highest values occurring in north-western and south-western Amazonia. For all underlying wood density maps, simulations using M2-4 display similar distributions of vegetation carbon to the control JULES output, while M1 causes total dieback. The main effect of using M2-4
260 is a change in the absolute values of vegetation carbon. Simulations using M3 closely match the control results (Figs. 3d,h,l), whereas those using M2 produce the lowest non-zero values, as expected, since the M2 mortality values are the highest after M1 (as shown in Fig. 2 and Table 2).

The new mortality configurations shift the mean vegetation carbon and add up to 16 MgCha^{-1} of "additional spatial variation" (ϕ, equation 2), 9.5% of the mean vegetation carbon in the control result. The second effect is illustrated in Fig. 4, which
265 shows the spatial variation additional to that already present in the control simulation for the nine mortality configurations with
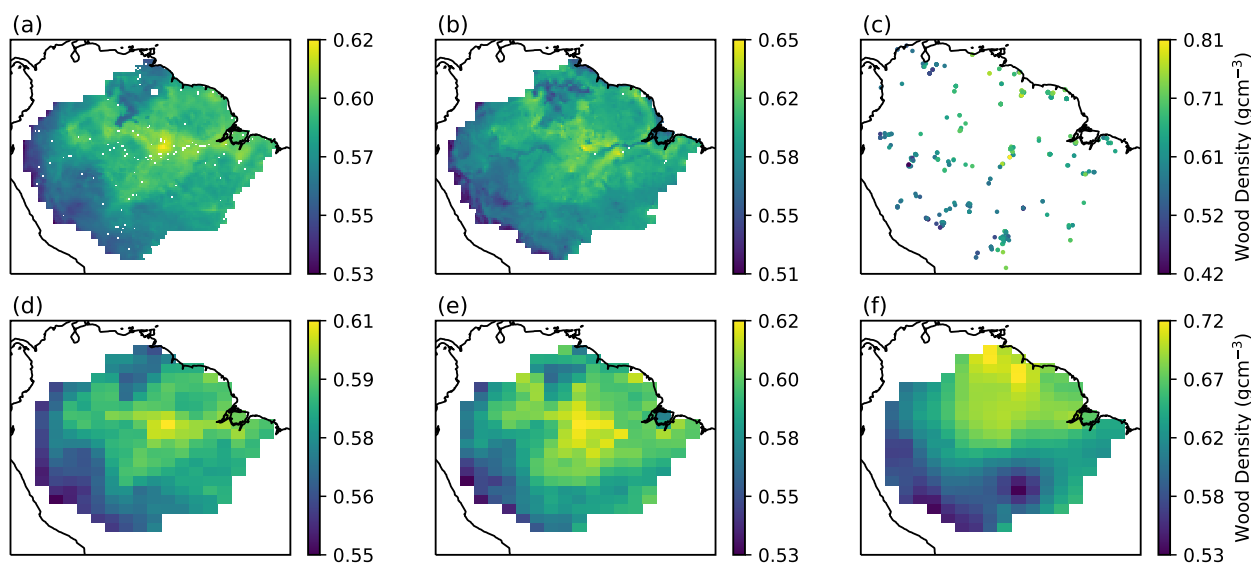
Figure 1. Wood density across the Amazon forest. (a) is a 25 km resolution map derived from the unweighted mean wood densities of species occurring in each grid cell, estimated using SDMs (called the "SDM-based" map). (b) is a 25 km resolution map, predicted using a regularised RF model with climate and disturbance as predictors (called the "RF-based" map). The points in (c) show the locations of 414 forest plots from (Mitchard et al., 2014), and the colour of each point reflects the basal area weighted mean wood density. (d) and (e) are the regridded versions of (a) and (b), respectively. (f) is a kriged map of wood density interpolated from the 414 plots shown in (c).

non-zero results. A positive change in vegetation carbon compared to the mean over all grid cells is shown by red grid cells and a negative change is shown in blue. The results using M3 (Figs. 4b,e,h) have the least change in the distribution of vegetation carbon, while those using M2 have the most. Of the three wood density maps, the kriged maps (Figs. 4g–i) provide the most extra variation because they include a greater range of wood density values. The most pronounced change is an increase in

270 the central-north and decrease in the central-south, in broad alignment with the gradient of mortality produced from the kriged wood density maps. Meanwhile, the change in the difference between south-eastern vegetation carbon and the mean is far less pronounced.

3.3 Model evaluation

The distributions of vegetation carbon in simulations with spatially explicit mortality improve on the simulation with homoge-

275 neous mortality, but do not yet fully capture the observed trends across the Amazon. This is seen in difference maps between simulations using M2-4 with the SDM-based, RF-based and kriged wood density data and an observational dataset, in Fig. 5. The control simulation and that using M3 largely overestimate vegetation carbon, except in the north-east. All simulations
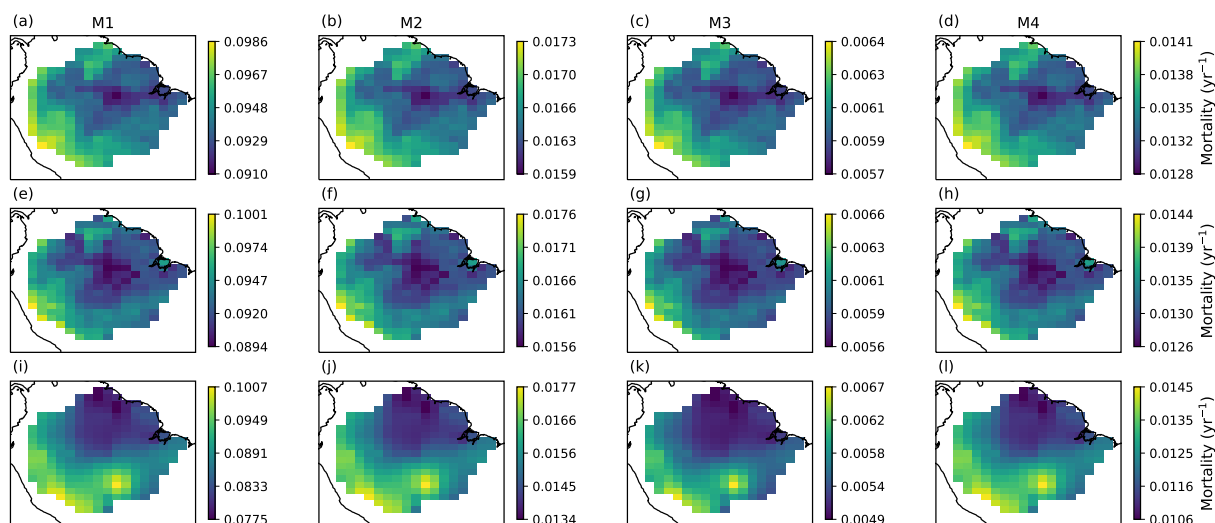
Figure 2. Mortality rates across Amazonia, calculated by the four different equations relating wood density to mortality listed in Table 1. (a), (e) and (i) use M1, (b), (f) and (j) use M2, and so on for the other two columns. (a) to (d) are calculated from the map of wood density in Fig. 1d, while (e) to (h) use the wood density map in Fig. 1e, and (i) to (l) use the kriged map in Fig. 1f. Note the different scale for each figure.

Table 2. The mean and standard deviation of mortality rates (in units per year) across Amazonia for the 12 new mortality configurations.

Mortality Model	Wood Density Map	Mean Mortality $\pm$ SD
M1	Occurrence	0.0945 ± 0.0015
M1	Observation	0.0933 ± 0.0021
M1	Kriged	0.0878 ± 0.0058
M2	Occurrence	0.0166 ± 0.0003
M2	Observation	0.0163 ± 0.0004
M2	Kriged	0.0153 ± 0.0011
M3	Occurrence	0.0060 ± 0.0001
M3	Observation	0.0059 ± 0.0002
M3	Kriged	0.0056 ± 0.0004
M4	Occurrence	0.0134 ± 0.0003
M4	Observation	0.0132 ± 0.0003
M4	Kriged	0.0123 ± 0.0010

using M2 and M4 overestimate in the arc of deforestation and the north-west. Vegetation carbon is underestimated from the north-east across to central Amazonia, especially in French Guiana and north-eastern Brazil. The statistical comparison in
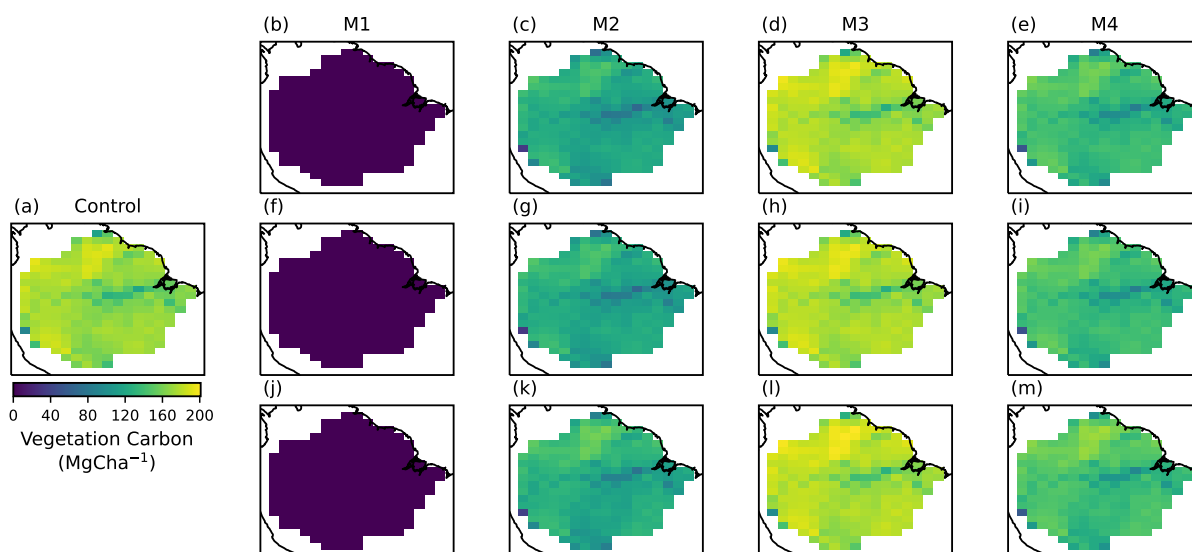
Figure 3. Maps of vegetation carbon for the present day (averaged 2008–2017) simulated by JULES. (a) shows the result from the original JULES configuration with a homogeneous mortality rate. (b) to (m) show the vegetation carbon simulated when spatially explicit mortality rates, based on a relationship with wood density, were included in JULES. (b), (f) and (j) used M1 to calculate the input mortality rates, (c), (g) and (k) used M2, and so on for the other two columns (mortality equations are found in Table 1). The mortality rates used for the simulations in (b) to (e) were calculated from the map of wood density in Fig. 1d, while (f) to (i) used the map in Fig. 1e, and (j) to (m) used the kriged map in Fig. 1f.

280 Table 3 shows that the bias is lowest for the configuration with M2 and SDM-based wood density data (lower than the bias associated with the control by almost a factor of 10), and that the CRMSD and correlation coefficient are best for M4 with kriged wood density data. The latter configuration increases the correlation coefficient to 0.24 from a value of 0.17 for the control. The standard deviation of the regridded Avitabile data was 35 MgCha^{-1}, most closely matched by the standard deviation of the results using M4 with kriged wood density (15 MgCha^{-1}). The new simulations perform similarly when compared
285 to vegetation carbon derived from the ESA CCI Biomass product (Fig. B2), though underestimation in the north-east is less pronounced and the correlation coefficient is increased in all cases (Table B1).

Overall, M2 and M4 with the kriged wood density data best replicate observations. The main improvement is a large reduction in bias, along with an increase in correlation and a reduction in the CRMSD. Although the mean values of simulated vegetation carbon in the Amazon are much improved by the new mortality schemes, the new mortality fields are less effective
290 at redistributing the modelled vegetation carbon across the region to better match observations.
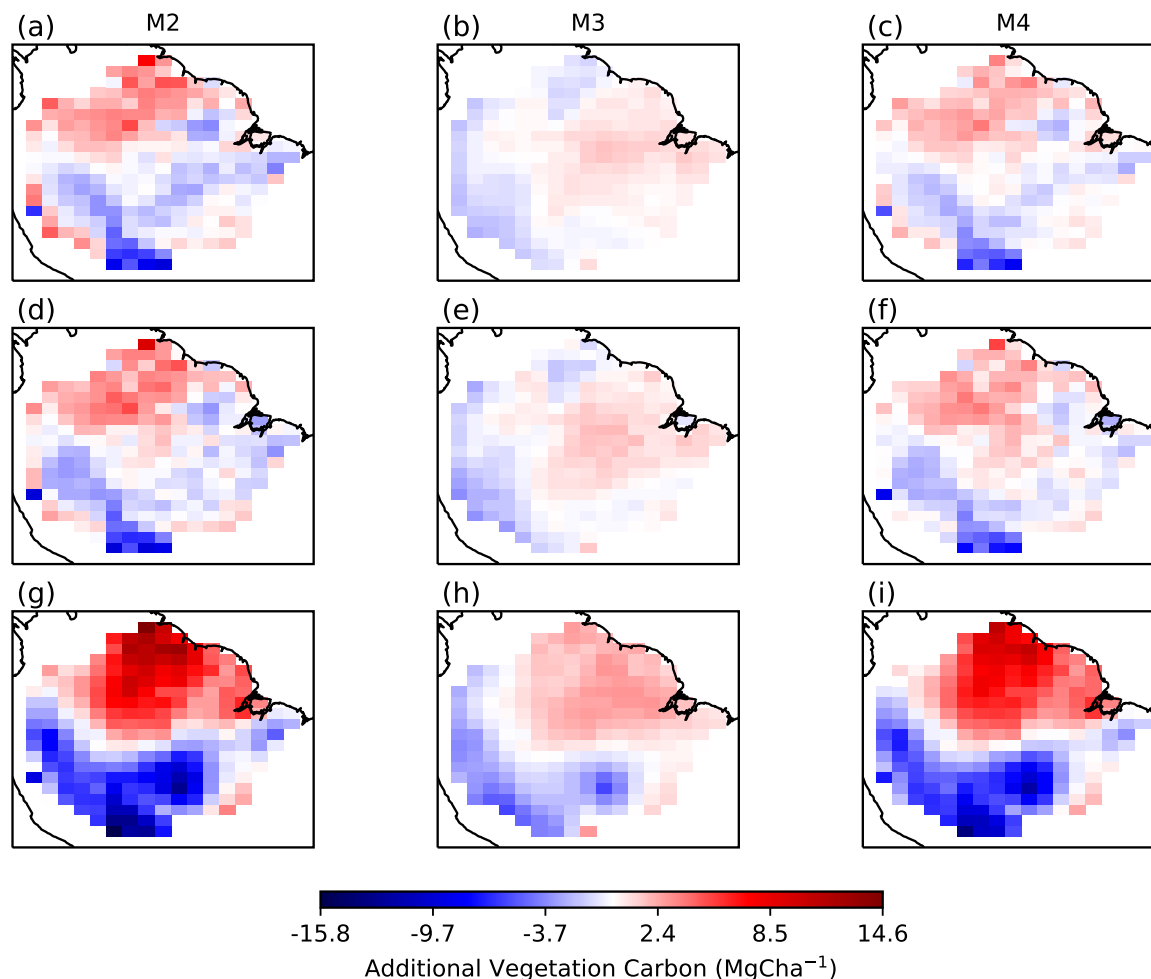
Figure 4. The additional spatial variation (ϕ) in simulated vegetation carbon resulting from the use of spatially-explicit mortality rates in JULES. Grid cells where the vegetation carbon increased compared to the mean across all grid cells when spatially explicit mortality rates were used in JULES are shown in red. Similarly, grid cells where the vegetation carbon decreased compared to the mean are shown in blue. Results are for the present day (averaged 2008–2017). (a), (d) and (g) use M2, and so on for the other two columns. (a) to (c) used mortality rates calculated from the map of wood density in Fig. 1d, while (d) to (f) used the map in Fig. 1e, and (g) to (i) used the kriged map in Fig. 1f.

Assuming that mortality is the sole predictor of vegetation carbon, an experiment was conducted using the linear fit in Fig. 6a to back-calculate the mortality rates required to reproduce the Avitabile map. Mortality rates ranging from the impossible value of -0.001 yr^{-1} to 0.0356 yr^{-1} are needed to capture the observed range of vegetation carbon. The high observed vegetation carbon in the north-east necessitates the negative mortality rates. The inferred mortality maps were then used to back-calculate the required wood density distributions according to the three non-zero wood density – mortality equations (Figs. 6b–d). The
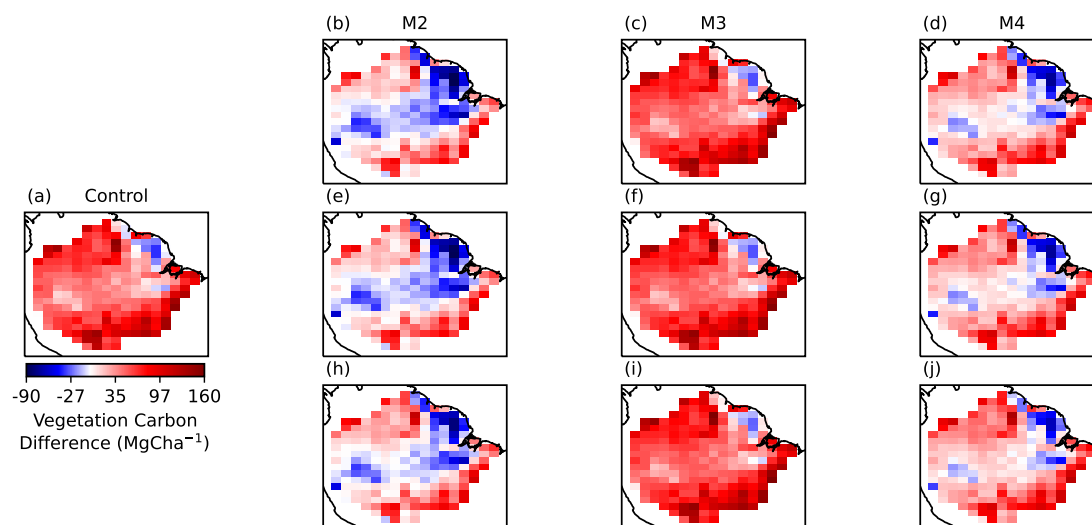
Figure 5. The difference between the simulated vegetation carbon for present day (averaged 2008–2017) and the observed vegetation carbon, derived from a fused biomass map based on remote sensing data (Avitabile et al., 2016). (a) shows the difference between the original JULES configuration with homogeneous mortality and the observations. The equations used to create the mortality data for the remaining simulations are indicated in the column titles. The mortality maps used in (b) to (d) are calculated from wood density map in Fig. 1d, while (e) to (g) use the wood density map in Fig. 1e, and (h) to (j) use kriged wood density in Fig. 1f.

outlying values in the north-east in Fig. 6c were caused by the low back-calculated mortality rates. M2–4 predict high wood densities in the north-east, aligning with areas of high observed vegetation carbon (Fig. B1). On the other hand, very low, and even negative wood densities are predicted at the forest fringes, notably in the arc of deforestation; these areas show low vegetation carbon in the observed map.

4 Discussion

4.1 Analysis of the mortality maps

4.1.1 Wood density – mortality equations

In a large assessment of long term RAINFOR plots across the Amazon, Esquivel-Muelbert et al. (2020) found mean mortality rates ranging from 0.028 yr^{-1} in the southern Amazon and 0.022 yr^{-1} in the western Amazon to 0.013 yr^{-1} and 0.014 yr^{-1} in the northern and central-eastern regions, respectively. While M2 and M4 produce mean mortality rates similar to these observations (e.g. 0.017 yr^{-1} and 0.013 yr^{-1} using the SDM-based map, as shown in Table 2), none of the mortality maps

Table 3. Statistical comparison of the JULES simulations (with different mortality configurations) of vegetation carbon with the observational Avitabile map. The absolute bias (MgCha^{-1}), CRMSD (MgCha^{-1}), Pearson correlation coefficient and standard deviation (MgCha^{-1}) of the simulated data are shown.

Mortality Model	Wood Density Map	Absolute Bias	CRMSD	Correlation Coefficient	Standard Deviation
Control	n/a	56.4	35.58	0.165	13.1
M1	Occurrence	112.3	35.31	0.071	0
M1	Observation	112.3	35.31	0.071	0
M1	Kriged	112.3	35.31	0.071	0
M2	Occurrence	6.1	35.81	0.163	14.0
M2	Observation	7.2	35.75	0.167	14.0
M2	Kriged	12.5	35.01	0.229	14.7
M3	Occurrence	61.4	35.41	0.174	12.8
M3	Observation	61.9	35.4	0.174	12.8
M3	Kriged	63.9	35.03	0.202	12.7
M4	Occurrence	22.6	35.62	0.172	13.7
M4	Observation	23.6	35.57	0.175	13.7
M4	Kriged	28.4	34.83	0.235	14.2

reproduce such a high degree of spatial variation. Esquivel-Muelbert et al. report a two-fold variation in *regional* mean mortality rates, while the most variation achieved in Fig. 2 is a 37% increase from the lowest to the highest mortality *grid cells*, for the kriged map with M4 (Fig. 2l).

310   The main differences in the simulations from the four wood density – mortality equations originate in their differing mean mortality rates and the range of mortality rates generated. M1 produced mean mortality rates as high as 0.0945 yr^{-1}, far higher than observations (Lugo and Scatena, 1996; McDowell et al., 2018; Esquivel-Muelbert et al., 2020), causing total dieback in the simulations. This is likely because M1 was designed to reflect the mortality rates of early successional species as well as late successional species (Moorcroft et al., 2001). Meanwhile, M3 gave results very similar to the case with homogeneous

315   mortality. This is because M3 produces a mean mortality rate close to the original constant rate used in JULES, and only 12% of the observed range of mean mortality rates between different Amazonian regions. The small range simulated by this equation may be due to the relatively small number of species it was based on. Additionally, almost half of the species were from the non-Amazonian *Dipterocarpaceae* family and evidence suggests that the strength of the wood density – mortality relationship depends on family (Kraft et al., 2010). Nonetheless, this equation may prove more suitable for regions with lower

320   wood density values because its non-linearity means that the rate of change of mortality with wood density is larger at low wood densities.
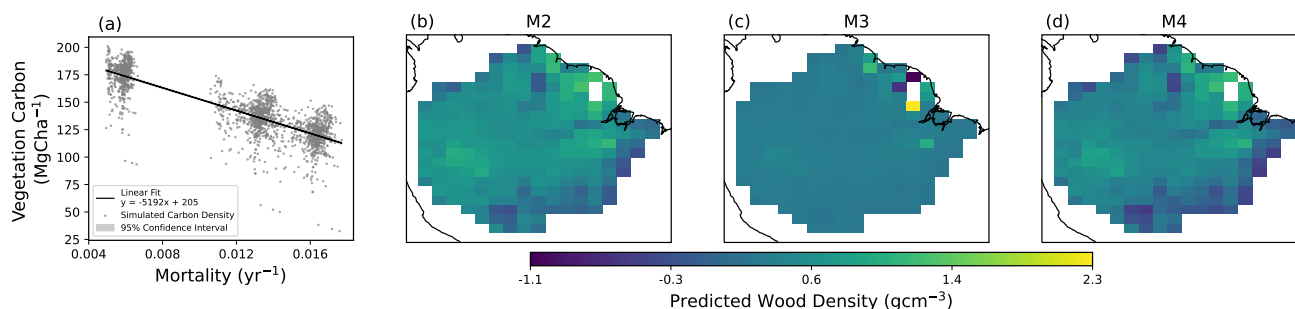
Figure 6. (a) Linear trend ($R^2 = 0.73$, p < 0.01) between simulated vegetation carbon and the mortality rates of the corresponding grid cells. (b) to (d) show the wood density data which would be needed to reproduce the observed vegetation carbon distribution in the Avitabile map (Avitabile et al., 2016) if mortality is calculated using the equations in the figure titles. The white cells in (c) are masked because of the negative mortality rates predicted by the regression in (a).

The spatial variation in mortality rates, and consequently in vegetation carbon, is higher using M2 and M4. M2 was directly fitted to data from 364 species in 59 families, possibly explaining the wider range of mortality rates it produces. M4 provides a similar range of mortality rates, and is indirectly based on wood density data, as the linear coefficient was tuned to reproduce

325 observations of AGB and other variables when used in the TROLL DGVM (Maréchaux and Chave, 2017). M4 is used as a background mortality rate in TROLL, whose mortality scheme also includes terms for carbon starvation and treefall, processes not included in JULES-TRIFFID. Though wood density is thought to relate to many aspects of mortality, the wood density – mortality link is insufficient to capture the total variation of mortality rates across Amazonia. This is due to missing mortality processes, especially in human modified forests, which will be discussed later. But a secondary cause is that the wood density

330 – mortality relationships derived by regressions are weakened by the dilution effect. The slopes of these regressions are biased towards zero because of the substantial noise in the wood density and mortality data.

The maximum wood density value used in M1 and M4 affects the gradients of these equations. The maximum community-averaged wood density could be even lower than the 1.25 gcm^{-3} used in this study. However, as shown by the dashed lines in Fig. A1, the gradient of M4 is very similar to that of M2 when a lower maximum wood density of used, so would likely give

335 similar results. M1 produced unrealistically high mortality rates at both values of maximum wood density. Therefore it can be concluded that the choice of ρ_{max} did not affect the conclusions of this research.

4.1.2 Wood density data

Figure 4 demonstrates that the source of wood density data strongly impacts the extra spatial variation in vegetation carbon. Furthermore, there is potential to capture much of the observed variation in vegetation carbon by capturing gradients of wood

340   density (as shown by Fig. 6). It must be stated that the distribution of vegetation carbon in the Amazon forest is controlled by more than solely wood density and mortality, as discussed in Sect. 4.3. A robust model would include these processes as well as accurately reflecting the spatial variation of mortality rates. Nonetheless, the greater spatial variation in vegetation carbon simulated when a higher range of wood density values is used to calculate mortality fields (comparing Fig. 4a and Fig. 4g, for example) shows potential for further improvements if the full range of observed wood density is accurately accounted for.

345   The SDM-based map has the smallest range due to several factors: the grid cells of the original map represent community-wide averages at a 25 km scale, which are then regridded to a much coarser scale; the averages are not weighted by species abundance, causing further smoothing; and species occurrence is predicted by SDMs, which give potential and not actual distributions. The first point is inescapable, as JULES is not an individual based model and requires a degree of averaging for all input parameters. The regridding process used in the SDM- and RF-based maps reduced the wood density range by 28% and

350   36%, respectively. There is a trade-off between the accuracy of the regridded map (i.e. the faithful representation of the source cells by the new, larger grid cells) and its spatial heterogeneity. The area weighted regridding method chosen for this study favours accuracy. To address the second point, spatially explicit species abundance data to weight the community mean would be needed. Even though SDM-based maps generated by only including the 227 hyperdominant Amazonian species produced similar results, this did not account for spatial variation in the dominance of these species, 73% of which are dominant within

355   only one or two regions (Ter Steege et al., 2013). The Amazon Tree Diversity Network (Ter Steege et al., 2013) provides abundance information for 1170 plots across Amazonia, and could be used in future to weight wood density pixels. The new Brazilian National Forest Inventory (de Freitas et al., 2009) could also provide opportunities in this respect. Finally, the use of SDMs smooths the community mean wood density because SDMs predict potential species occurrences in a given location. These differ from actual species occurrences if dispersal limitations, inter-specific competition and non-equilibrium dynamics

360   are not considered (Maréchaux et al., 2021).

      The RF-based wood density map, derived from predictions by a regularised RF model, removes the challenges associated with using SDMs, but does not greatly extend the wood density range. In contrast, the kriged wood density map clearly provides additional spatial variation in vegetation carbon, which better matches observations (Table 3). This method is based on wood density data weighted by species basal area for each plot. The kriging utilised all 414 plots available, meaning that

365   some 1.875° by 1.25° grid cells contained several plots representing data collected over 1 ha. When all but one randomly selected plot was filtered out in each grid cell, the results of the kriging remained relatively stable, though the low wood density patch in the south-east was removed. The standard deviation of the kriged wood density map was very similar when all plots were considered (0.048 gcm^{-3}) to when only one plot per grid cell was considered (on average, 0.044 gcm^{-3}). The wider wood density range in the kriged map is more realistic, given that Quesada et al. (2012) found volume weighted wood density

370   plot averages from 0.49 to 0.73 gcm^{-3} in the Amazon. However, as noted in (Johnson et al., 2016), kriging is unsuitable for describing localised heterogeneity. The accuracy of the kriging was also relatively low, with R^2=0.35, and it was based on data from intact forests only. Explicitly including wood density data from human modified forests would further expand the wood density range by increasing the representation of low wood density, early successional species. It is possible that a combination

of the approaches used in the RF-based and kriged maps would be the best way forward, i.e. using a regularised RF model,
375   crucially including disturbance layers, trained on basal area weighted wood density pixels.

4.2   Challenges with observed vegetation carbon

A large part of the analysis of the best mortality configuration relies on a comparison with observations of vegetation carbon. The first challenge to note is that the observations include vegetation carbon in highly disturbed and secondary forests, whereas human land use change was not included in these JULES simulations. Nevertheless our investigation sheds light on the effec-
380   tiveness of wood density dependent mortality fields for improving the distribution of vegetation carbon for old growth forests, as will be discussed in Sect. 4.3.

The Avitabile fused map was created to correct the problems in two previous biomass maps based on remote sensing, including the use of continent-wide height allometries which contributed to underestimation in the north-east (Mitchard et al., 2014). It was found to have a lower root mean square error than the two input maps and nearly zero bias. A comparison of
385   existing biomass maps (Zhang et al., 2019) for South America shows that the Avitabile map is in broad agreement with other datasets (Hu et al., 2016; Zhang et al., 2019). The uncertainties in the eastern Amazon are still relatively large ($\sim$30 MgCha^{-1}) and this estimate does not include the uncertainty associated with classifying the errors in the input map, potentially a large contribution (Avitabile et al., 2016). The lack of reference data from disturbed forests in the Avitabile et al. study may cause errors in the arc of deforestation, where this map records more carbon than the ESA CCI product (see Fig. B1). Future analysis
390   could consider comparing JULES outputs to the upcoming GEDI L4B map of AGB, which will incorporate a larger number of observations of the tropics than used in the sources of the Avitabile map (Dubayah et al., 2020).

On the whole, the Avitabile map was deemed more suitable than other remote sensing products, which tend to saturate at high biomass values (Turner et al., 2006; Le Toan et al., 2020). However, the ESA CCI Biomass product was also used to benchmark these simulations as a potentially more accurate source for disturbed, low carbon regions. The new simulations have stronger
395   correlations with the ESA CCI observed map than with the Avitabile map, and a smaller difference in correlation between the best new result and the control simulation. Spatial patterns of over- and underestimation are similar, though underestimation in the north-east is less pronounced.

4.3   Missing spatial variation

It was expected that adding a wood density dependent mortality term would improve the representation of Amazonian vege-
400   tation carbon in JULES, since previous research has shown that mortality rates (Malhi et al., 2015; Johnson et al., 2016) and wood density (Baker et al., 2004) are good predictors of biomass. This paper has shown that adding spatially varying mortality rates, dependent on wood density, into JULES improves predictions for vegetation carbon by reducing the bias to around 10% of its original value and by increasing the correlation with observations by around 40%. Future work will aim to improve the accuracy of predictions even further by including other missing processes that impact vegetation carbon. We propose that
405   the remaining "missing" variation originates from non-mortality mechanisms like NPP and carbon allocation (i.e. variation in carbon input) and missing mortality processes (variation in carbon losses).

The results in Fig. 6 give a good indication of where the "missing" processes above are most important in the Amazon. Individual species measured in tropical South America have wood densities from 0.10 to 1.21 gcm^{-3} (Zanne et al., 2009), which sets extreme bounds for feasible values of wood density, though a more realistic range would be smaller due to community av-
410   eraging. While the wood density pixels back-calculated from M2–4 are predominantly within the range for individual species, key regions of unrealistic values lie in the north-east and south-east. The high wood densities (and even negative mortality rates) required in the north-east suggest that low mortality rates cannot capture the large biomass stores there. This is where variation in the carbon input to the forest (e.g. through NPP gradients or carbon allocation) is likely especially important for modelling vegetation carbon. Conversely, the negative wood density pixels predicted in the south-east suggest that additional
415   sources of tree mortality are not accounted for by the wood density – mortality link. A key missing factor here is likely human disturbance and land use change Bullock et al. (2020).

4.3.1   Non-mortality sources of variation

In the JULES simulations, regions of high simulated NPP correlated well with regions of high simulated vegetation carbon, as is the case in many DGVMs (Johnson et al., 2016). However, in reality there is a weak (Johnson et al., 2016) and non-
420   linear relationship between above ground NPP and vegetation carbon in the tropics (Keeling and Phillips, 2007) and the two may even be negatively correlated in highly productive forests. Delbart et al. (2010) found that modelling mortality rates as proportional to NPP$^{1.32}$ allowed the ORCHIDEE model to better represent the pattern of biomass across old growth Amazonian forests. The authors suggest that productivity-mortality-biomass covariation is linked to soil properties; physical soil properties are correlated with mortality rates and soil fertility, particularly soil phosphorus concentration, is correlated with
425   NPP (Malhi et al., 2004; Quesada et al., 2012). A study using a canopy photosynthesis model calibrated for Amazonia has found that canopy phosphorus concentrations drive variations in GPP, which play a large role in predicting variations in wood production (Mercado et al., 2011). The fertile soils in the south-west are productive, favouring fast growing species with low wood density (Quesada et al., 2012). In contrast, soils in central and eastern Amazonia have lower fertility and good physical properties (Quesada et al., 2010), promoting slow growth (Quesada et al., 2012), low mortality rates (Johnson et al., 2016)
430   and consequently selecting for tall (Feldpausch et al., 2011), high wood density trees which store a lot of carbon. Therefore the addition of the phosphorus cycle to land surface models, including JULES (Nakhavali et al., 2021) and ORCHIDEE (Sun et al., 2021), is a very promising avenue for exploring vegetation carbon variation.

The fact that wood density-dependent mortality did not explain all spatial variation in vegetation carbon reflects results from field measurements. As previously mentioned, Baker et al. (2004), found that wood density explained at most 45% of the
435   variation in AGB across 56 Amazonian mature forest sites. The basal area of large trees was another important predictor of AGB variation between these plots, but it did not vary significantly between regions. Quesada et al. (2012) used a broader range of sites to report higher basal areas in forests in north-east than in south-west Amazonia, in a negative relationship with soil fertility and a positive relationship with average dry season precipitation. High AGB plots had higher average wood density, but plots with lower AGB had varying wood density, and here basal area strongly correlated with AGB. Stand basal area was
440   mainly controlled by the basal area per tree, showing that the stem diameter distribution of trees across the Amazon was an

important predictor of AGB, and was at least partially uncoupled from wood density. Additionally, allometric equations for AGB require both stem diameter and tree height as well as wood density to accurately predict AGB (Chave et al., 2014), and evidence suggests that wood density does not correlate with tree height (Francis et al., 2017). The allometry between stem diameter and tree height also depends on region and climate, with trees in the Guiana shield displaying greater heights for
445   a given diameter than in the wider Amazon (Feldpausch et al., 2011), likely affecting carbon storage (Gora and Esquivel-Muelbert, 2021). Indeed, differences tree height help explain the regional variation AGB in Amazonia (Nogueira et al., 2008; Feldpausch et al., 2012). Feldpausch et al. (2011) postulate that the regional differences in height allometry are in part due to the effect of geological events in the last glacial maximum on species composition. Height is allowed to vary in JULES, but future work should address whether realistic height distributions are simulated, and whether the allometric relationships used
450   to calculate it should vary in space.

   Wood density is positively correlated with biomass (Quesada et al., 2012), and there is mixed evidence linking high wood density and slow growth (Nascimento et al., 2005; Wright et al., 2010; Francis et al., 2017). Wood density could act as a bridge connecting NPP and mortality in a positive relationship in JULES, capturing the wood economics spectrum more fully. As such, coupling high wood density with increased woody allocation and slow growth may amplify the extra spatial variation
455   between the south-western and eastern Amazon. More data are needed to fully understand the link between wood density and carbon allocation, but one example shows that among South African tree species, high wood density species have a lower leaf:woody biomass ratio than low wood density species (Mensah et al., 2016).

4.3.2   Missing mortality

As previously mentioned, the wood density – mortality relationship is likely linked to stem mechanical strength, reduced
460   risk of drought-induced embolism and possibly resistance to pathogen attack (Chave et al., 2009). However, not all mortality processes are captured in this relationship; Kraft et al. (2010) find that wood density variation explains on average 40% of mortality variation in a pantropical analysis.

   The tree death is more commonly caused by windthrow in the dynamic, western Amazon (Negrón-Juárez et al., 2018; Esquivel-Muelbert et al., 2020). This mode of mortality may be captured in the low wood densities found in the region (Fig. 1).
465   In the eastern-central and southern Amazon, Esquivel-Muelbert et al. (2020) report that a physiological cause of death, such as stress, senescence or hydraulic failure, is more likely. It is almost certain that fires, intensified by anthropogenic disturbance and extreme drought play a large role in the spatial variation of mortality in the south-east too, especially at forest edges (Brando et al., 2014). The mortality mechanisms dominating in these highly disturbed regions are very different from those in intact forests, from which M2–4 were derived. For example, high wood density trees are often removed in selective logging (Gaui
470   et al., 2019). When grid cells containing a high proportion of disturbed forest are removed from the analysis in Fig. C1, the bias and CRMSD of the simulations compared to observations are further reduced (see Table C1), though areas of error still remain in a belt from central-western to north-eastern Amazonia (Fig. C2).

   Intermediate wood density values are recorded in the arc of deforestation (Fig. 1), suggesting that the species mix is not, on average, particularly drought-tolerant, given that high wood density is correlated with resistance to drought-induced mortality

475 (Greenwood et al., 2017). It could be that climate extremes in the south-east and north (Brando et al., 2014) (such as the record breaking drought and temperature anomalies recorded in the 2015 El Niño event (Jiménez-Muñoz et al., 2016)) are exceeding the drought tolerances of the species present, which were selected under historical levels of moisture stress. Wood density is a non-plastic trait (Chave et al., 2006), making it plausible that mortality rates are higher than the wood density – mortality link would suggest.

480 It has been suggested that repeated droughts in north-eastern Amazonia during the Holocene shifted species composition towards more drought-tolerant communities (Maréchaux et al., 2015). As increasing present day water stress starts to trigger composition change from lower to higher wood density species and/or to lower-statured species (Esquivel-Muelbert et al., 2019), carbon stocks and dynamics could change dramatically. In other locations, where the Amazon is becoming more dynamic with increasing growth and mortality rates, species composition is shifting towards faster growing genera (Phillips et al.,

485 2008). Therefore, making spatially explicit *and* dynamic mortality maps which track potential wood density change could be an important avenue to follow in future JULES development. This could be linked to the addition of tree demography into JULES (through the Robust Ecosystem Demography DGVM (Argles et al., 2020)), allowing multiple coexisting successional stages (potentially with different wood density distributions) to more accurately represent composition change. It would also be informative to test whether the simulated vegetation carbon distribution could be improved if average observed mortality

490 rates for each grid cell are input directly into the model, without the wood density step. For example, spatially varying woody residence times across Amazonia have been included in an average-individual model, with kriged data from a set of 34 1° x 1° grid cells, achieving some success (Castanho et al., 2013).

5 Conclusions

This work has shown that it is possible to include spatially explicit mortality rates for tropical tree PFTs in large-scale DGVMs,

495 despite the lack of tree mortality data with sufficient range and resolution for modelling. Mortality maps can instead be generated using relationships with more easily measured plant traits; a particularly useful trait is wood density, used here to create maps of mortality across Amazonia.

This research highlights that a wide range of mortality rates are needed to correctly model vegetation carbon in Amazonia, particularly in disturbed forests and in the Guiana shield. For the JULES land surface scheme employed above, this emphasises

500 the importance of including mortality due to fire and drought, and of simulating early successional stages. The work also suggests that non-mortality influences on vegetation carbon are important, such as variations in productivity from the phosphorus cycle, and variations in carbon allocation.

Implementing the improvements to PFT mortality schemes in vegetation models outlined in this paper would expand the potential for accurately modelling the spatial distribution of vegetation carbon and the size of the vegetation carbon sink. This

505 method also opens up several avenues for further improvements, such as coupling mortality to growth rates, adding spatial diversity to drought and fire responses, and adding temporal dynamics to mortality rates via trait composition change.

Code and data availability. JULES output for the 12 mortality configurations and control configuration, for present day, has been archived at https://doi.org/10.5281/zenodo.6388019. The 12 mortality maps and the kriged wood density map are also found in this repository.

510   The SDM- and RF- based wood density maps have not yet been made publicly accessible because their creators, FJF and JC and collaborators, are preparing to publish them separately in upcoming manuscripts.

The JULES code and the Rose suite (suite u-cg769) for these simulations is available on the Met Office Science Repository System (MOSRS; https://code.metoffice.gov.uk/ trac/jules). Free registration is required to access MOSRS.

Appendix A
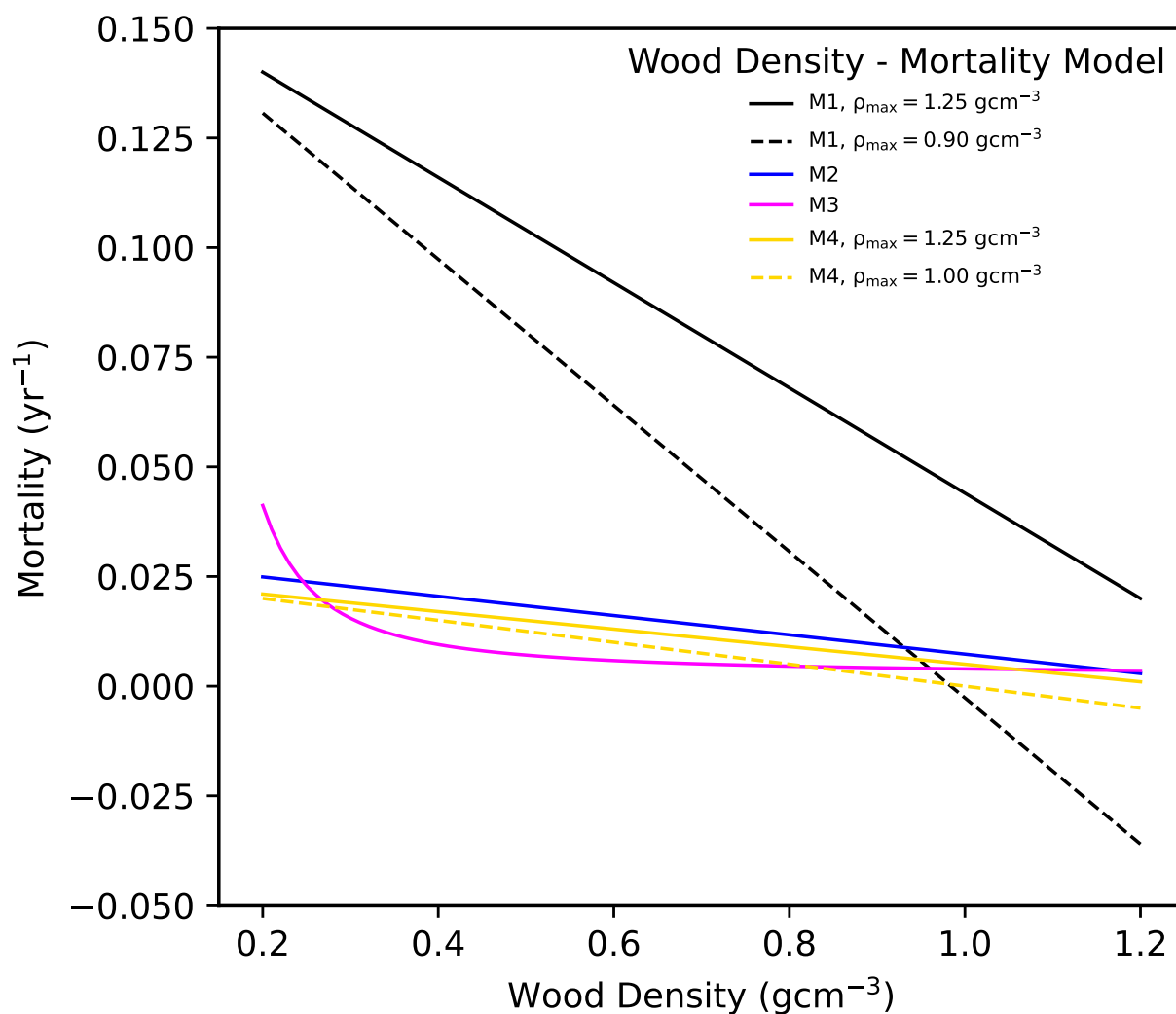
Figure A1. A comparison of the four equations describing the wood density – mortality relationship used in this paper. Also included are the original versions of M1 and M4, which have different maximum wood density (ρ_{max}) values, as indicated in the legend. The wood density data are simulated in this figure.

Appendix B
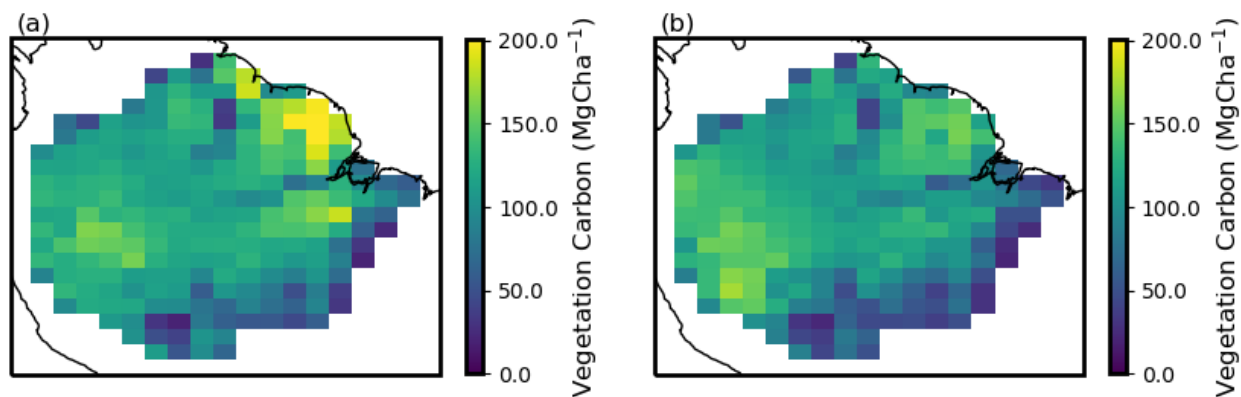
Figure B1. Observational maps of vegetation carbon. (a) is derived from a map produced by Avitabile et al. (2016) which combines remote sensing and forest inventory data. (b) is derived from the ESA CCI Biomass product (Santoro and Cartus, 2021). Both have been regridded to match the resolution of the JULES driving data.
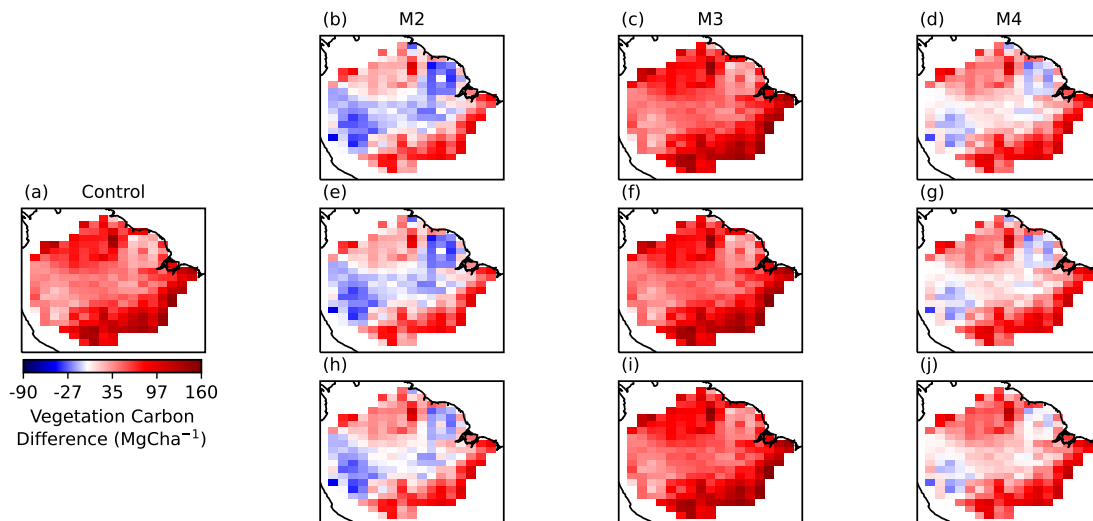
Figure B2. The difference between the vegetation carbon for present day simulations (averaged 2008–2017) and that derived from the ESA CCI Biomass product (Santoro and Cartus, 2021). (a) shows the difference between the original JULES configuration with homogeneous mortality and the observations. The models used to create the mortality data for the remaining simulations are indicated in the column titles. The mortality maps used in (b) to (d) are calculated from SDM-based wood density data, while (e) to (g) use RF-based wood density, and (h) to (j) use kriged wood density.

Table B1. Statistical comparison of the JULES simulations (with different mortality configurations) of vegetation carbon with the observational ESA CCI product. The absolute bias (MgCha^{-1}), CRMSD (MgCha^{-1}) and the Pearson correlation coefficient are shown.

Mortality Model	Wood Density Map	Absolute Bias	CRMSD	Correlation Coefficient
Control	n/a	64.3	33.37	0.263
M1	Occurrence	104.4	34.33	0.202
M1	Observation	104.4	34.33	0.202
M1	Kriged	104.4	34.33	0.202 .
M2	Occurrence	14.0	33.49	0.263
M2	Observation	15.1	33.46	0.265
M2	Kriged	20.4	33.19	0.29
M3	Occurrence	69.4	33.38	0.259
M3	Observation	69.9	33.37	0.26
M3	Kriged	71.8	33.17	0.275
M4	Occurrence	30.6	33.36	0.269
M4	Observation	31.6	33.34	0.27
M4	Kriged	36.4	33.03	0.296

515 **Appendix C**
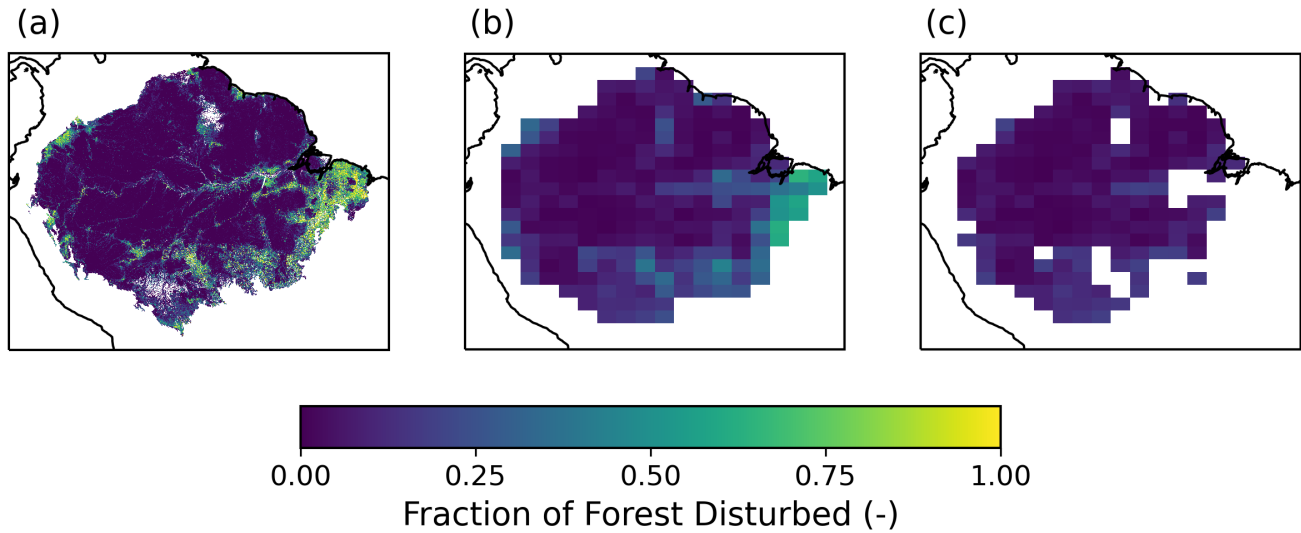
Figure C1. The fraction of the forest present in each grid cell that is disturbed. The total area of disturbed forest per grid cell is the sum of secondary and degraded forest area, and non forested areas are masked. (a) shows the original dataset at 1 km resolution. (b) shows the fraction of disturbed forest after regridding using the method in Sect. 2.3. (c) shows the remaining grid cells after those whose forested area is over 20% disturbed are removed.
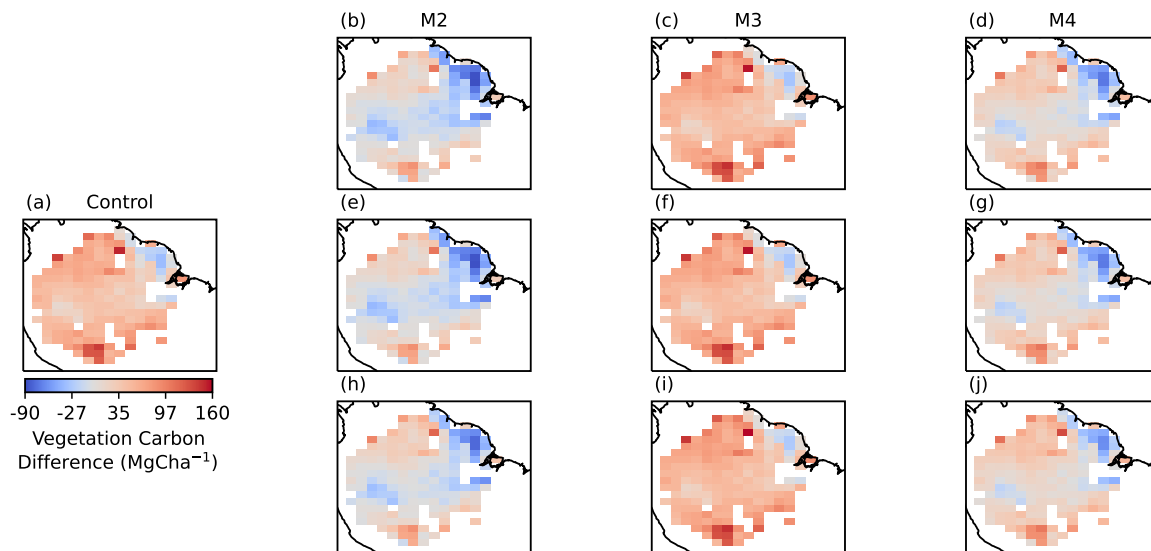
Figure C2. The difference between the vegetation carbon for the present day (averaged 2008–2017), simulated using different mortality configurations, and that derived from the Avitabile et al. map (Avitabile et al., 2016) in largely undisturbed forests. (a) shows the difference between the original JULES configuration with homogeneous mortality and the observational map. (b), (e) and (h) use mortality maps from M2, and so on for the other two columns. The mortality maps in (b) to (d) are calculated from the SDM-based map of wood density, while (e) to (g) use the RF-based wood density map, and (h) to (j) use the kriged wood density map.

Table C1. Statistical comparison of the control JULES simulation and the nine non-zero simulations of vegetation carbon with different mortality configurations *after highly disturbed forests are filtered out* and the vegetation carbon derived from the Avitabile map. The absolute bias (MgCha^{-1}), CRMSD (MgCha^{-1}) and Pearson correlation coefficient are shown.

Mortality Model	Wood Density Map	Absolute Bias	CRMSD	Correlation Coefficient
Control	n/a	48.6	30.57	0.124
M2	Occurrence	1.6	30.66	0.137
M2	Observation	0.5	30.60	0.139
M2	Kriged	4.9	29.73	0.232
M3	Occurrence	53.6	30.30	0.141
M3	Observation	54.2	30.29	0.141
M3	Kriged	56.1	29.80	0.190
M4	Occurrence	14.9	30.50	0.142
M4	Observation	16.0	30.45	0.145
M4	Kriged	20.8	29.57	0.236

Author contributions. LMM, SS and MH conceptualised the study and designed the methodology. MH performed the JULES modelling and data analysis with contributions from LMM, SS and MO. FJF and JC created the SDM-based and RF-based wood density maps/distributions. DF produced the map of disturbed forest fraction for Amazonia. MH wrote the manuscript with contributions from all authors.

Competing interests. The authors declare that they have no conflict of interest.

520 *Acknowledgements.* LMM acknowledges funding from the UK Natural Environment Research Council funding (UK Earth System Modelling Project, UKESM, Grant NE/N017951/1). FJF and JC were supported by the "Investissement d'Avenir" grants managed by the Agence Nationale de la Recherche (CEBA, ref. ANR-10-LABX-25-01; TULIP, ref. ANR-10-LABX-0041; ANAEE-France: ANR-11-INBS-0001). DF and SS were supported by ESA Climate Change Initiative RECCAP2 (contract no. 4000123002/18/I-NB).

References

Abatzoglou, J. T., Dobrowski, S. Z., Parks, S. A., and Hegewisch, K. C.: TerraClimate, a high-resolution global dataset of monthly climate and climatic water balance from 1958–2015, Scientific data, 5, 1–12, https://doi.org/10.1038/sdata.2017.191, 2018.

Argles, A. P., Moore, J. R., Huntingford, C., Wiltshire, A. J., Harper, A. B., Jones, C. D., and Cox, P. M.: Robust Ecosystem Demography (RED version 1.0): a parsimonious approach to modelling vegetation dynamics in Earth system models, Geosci. Model Dev., 13, 4067–4089, https://doi.org/10.5194/gmd-13-4067-2020, 2020.

Avitabile, V., Herold, M., Heuvelink, G. B., Lewis, S. L., Phillips, O. L., Asner, G. P., Armston, J., Ashton, P. S., Banin, L., Bayol, N., et al.: An integrated pan-tropical biomass map using multiple reference datasets, Glob. Change Biol., 22, 1406–1420, https://doi.org/10.1111/gcb.13139, 2016.

Baccini, A., Goetz, S., Walker, W., Laporte, N., Sun, M., Sulla-Menashe, D., Hackler, J., Beck, P., Dubayah, R., Friedl, M., et al.: Estimated carbon dioxide emissions from tropical deforestation improved by carbon-density maps, Nat. Clim. Change, 2, 182–185, https://doi.org/10.1038/nclimate1354, 2012.

Badger, A. M. and Dirmeyer, P. A.: Remote tropical and sub-tropical responses to Amazon deforestation, Clim. Dynam., 46, 3057–3066, https://doi.org/10.1007/s00382-015-2752-5, 2016.

Baker, T. R., Phillips, O. L., Malhi, Y., Almeida, S., Arroyo, L., Di Fiore, A., Erwin, T., Killeen, T. J., Laurance, S. G., Laurance, W. F., et al.: Variation in wood density determines spatial patterns in Amazonian forest biomass, Glob. Change Biol., 10, 545–562, https://doi.org/10.1111/j.1365-2486.2004.00751.x, 2004.

Best, M., Pryor, M., Clark, D., Rooney, G., Essery, R., Ménard, C., Edwards, J., Hendry, M., Porson, A., Gedney, N., et al.: The Joint UK Land Environment Simulator (JULES), model description–Part 1: energy and water fluxes, Geosci. Model Dev., 4, 677–699, https://doi.org/10.5194/gmd-4-677-2011, 2011.

Brando, P. M., Balch, J. K., Nepstad, D. C., Morton, D. C., Putz, F. E., Coe, M. T., Silvério, D., Macedo, M. N., Davidson, E. A., Nóbrega, C. C., et al.: Abrupt increases in Amazonian tree mortality due to drought–fire interactions, P. Natl. Acad. Sci. USA, 111, 6347–6352, https://doi.org/10.1073/pnas.1305499111, 2014.

Brienen, R. J., Phillips, O. L., Feldpausch, T. R., Gloor, E., Baker, T. R., Lloyd, J., Lopez-Gonzalez, G., Monteagudo-Mendoza, A., Malhi, Y., Lewis, S. L., et al.: Long-term decline of the Amazon carbon sink, Nature, 519, 344–348, https://doi.org/10.1038/nature14283, 2015.

Bullock, E. L., Woodcock, C. E., Souza Jr, C., and Olofsson, P.: Satellite-based estimates reveal widespread forest degradation in the Amazon, Glob. Change Biol., 26, 2956–2969, https://doi.org/10.1111/gcb.15029, 2020.

Cardoso, D., Särkinen, T., Alexander, S., Amorim, A. M., Bittrich, V., Celis, M., Daly, D. C., Fiaschi, P., Funk, V. A., Giacomin, L. L., et al.: Amazon plant diversity revealed by a taxonomically verified species list, P. Natl. Acad. Sci. USA, 114, 10 695–10 700, https://doi.org/10.1073/pnas.1706756114, 2017.

Castanho, A. D. A., Coe, M. T., Costa, M. H., Malhi, Y., Galbraith, D., and Quesada, C. A.: Improving simulated Amazon forest biomass and productivity by including spatial variation in biophysical parameters, Biogeosciences, 10, 2255–2272, https://doi.org/10.5194/bg-10-2255-2013, 2013.

Chave, J., Andalo, C., Brown, S., Cairns, M. A., Chambers, J. Q., Eamus, D., Fölster, H., Fromard, F., Higuchi, N., Kira, T., et al.: Tree allometry and improved estimation of carbon stocks and balance in tropical forests, Oecologia, 145, 87–99, https://doi.org/10.1007/s00442-005-0100-x, 2005.

560 Chave, J., Muller-Landau, H. C., Baker, T. R., Easdale, T. A., Steege, H. t., and Webb, C. O.: Regional and phyloge-
netic variation of wood density across 2456 neotropical tree species, Ecol. Appl., 16, 2356–2367, https://doi.org/10.1890/1051-
0761(2006)016[2356:RAPVOW]2.0.CO;2, 2006.

Chave, J., Coomes, D., Jansen, S., Lewis, S. L., Swenson, N. G., and Zanne, A. E.: Towards a worldwide wood economics spectrum, Ecol.
Lett., 12, 351–366, https://doi.org/10.1111/j.1461-0248.2009.01285.x, 2009.

565 Chave, J., Réjou-Méchain, M., Búrquez, A., Chidumayo, E., Colgan, M. S., Delitti, W. B., Duque, A., Eid, T., Fearnside, P. M., Goodman,
R. C., et al.: Improved allometric models to estimate the aboveground biomass of tropical trees, Glob. Change Biol., 20, 3177–3190,
https://doi.org/10.1111/gcb.12629, 2014.

Clark, D., Mercado, L., Sitch, S., Jones, C., Gedney, N., Best, M., Pryor, M., Rooney, G., Essery, R., Blyth, E., et al.: The Joint UK Land
Environment Simulator (JULES), model description—Part 2: carbon fluxes and vegetation dynamics, Geosci. Model Dev., 4, 701–722,
570 https://doi.org/10.5194/gmd-4-701-2011, 2011.

Cox, P. M.: Description of the "TRIFFID" dynamic global vegetation model, Hadley Centre technical note 24, 2001.

de Freitas, J. V., de Oliveira, Y. M., Brena, D. A., Gomide, G. L., Silva, J. A., et al.: The new Brazilian national forest inventory, in: McRoberts,
Ronald E.; Reams, Gregory A.; Van Deusen, Paul C.; McWilliams, William H., eds. Proceedings of the eighth annual forest inventory and
analysis symposium; 2006 October 16-19; Monterey, CA. Gen. Tech. Report WO-79. Washington, DC: US Department of Agriculture,
575 Forest Service. 9-12., vol. 79, 2009.

Delbart, N., Ciais, P., Chave, J., Viovy, N., Malhi, Y., and Toan, T. L.: Mortality as a key driver of the spatial distribution of aboveground
biomass in Amazonian forest: results from a dynamic vegetation model, Biogeosciences, 7, 3027–3039, https://doi.org/10.5194/bg-7-
3027-2010, 2010.

Dubayah, R., Blair, J. B., Goetz, S., Fatoyinbo, L., Hansen, M., Healey, S., Hofton, M., Hurtt, G., Kellner, J., Luthcke, S., et al.: The Global
580 Ecosystem Dynamics Investigation: High-resolution laser ranging of the Earth's forests and topography, Science of Remote Sensing, 1,
100 002, https://doi.org/10.1016/j.srs.2020.100002, 2020.

Esquivel-Muelbert, A., Baker, T. R., Dexter, K. G., Lewis, S. L., Brienen, R. J., Feldpausch, T. R., Lloyd, J., Monteagudo-Mendoza, A.,
Arroyo, L., Álvarez-Dávila, E., et al.: Compositional response of Amazon forests to climate change, Glob. Change Biol., 25, 39–56,
https://doi.org/10.1111/gcb.14413, 2019.

585 Esquivel-Muelbert, A., Phillips, O. L., Brienen, R. J., Fauset, S., Sullivan, M. J., Baker, T. R., Chao, K.-J., Feldpausch, T. R.,
Gloor, E., Higuchi, N., et al.: Tree mode of death and mortality risk factors across Amazon forests, Nat. Commun., 11, 1–11,
https://doi.org/10.1038/s41467-020-18996-3, 2020.

Feldpausch, T. R., Banin, L., Phillips, O. L., Baker, T. R., Lewis, S. L., Quesada, C. A., Affum-Baffoe, K., Arets, E. J., Berry, N. J., Bird, M.,
et al.: Height-diameter allometry of tropical forest trees, Biogeosciences, 8, 1081–1106, https://doi.org/10.5194/bg-8-1081-2011, 2011.

590 Feldpausch, T. R., Lloyd, J., Lewis, S. L., Brienen, R. J., Gloor, M., Monteagudo Mendoza, A., Lopez-Gonzalez, G., Banin, L.,
Abu Salim, K., Affum-Baffoe, K., et al.: Tree height integrated into pantropical forest biomass estimates, Biogeosciences, 9, 3381–3403,
https://doi.org/10.5194/bg-9-3381-2012, 2012.

Francis, E. J., Muller-Landau, H. C., Wright, S. J., Visser, M. D., Iida, Y., Fletcher, C., Hubbell, S. P., and Kassim, A. R.: Quantifying
the role of wood density in explaining interspecific variation in growth of tropical trees, Global Ecol. and Biogeogr., 26, 1078–1087,
595 https://doi.org/10.1111/geb.12604, 2017.

Friedlingstein, P., O'Sullivan, M., Jones, M. W., Andrew, R. M., Hauck, J., Olsen, A., Peters, G. P., Peters, W., Pongratz, J., Sitch, S., et al.:
Global carbon budget 2020, Earth Syst. Sci. Data, 12, 3269–3340, https://doi.org/10.5194/essd-12-3269-2020, 2020.

Fu, X. and Meinzer, F. C.: Metrics and proxies for stringency of regulation of plant water status (iso/anisohydry): a global data set reveals coordination and trade-offs among water transport traits, Tree Physiol., 39, 122–134, https://doi.org/10.1093/treephys/tpy087, 2019.

600 Fyllas, N. M., Patiño, S., Baker, T. R., Bielefeld Nardoto, G., Martinelli, L. A., Quesada, C. A., Paiva, R., Schwarz, M., Horna, V., Mercado, L., et al.: Basin-wide variations in foliar properties of Amazonian forest: phylogeny, soils and climate, Biogeosciences, 6, 2677–2708, https://doi.org/10.5194/bg-6-2677-2009, 2009.

Galbraith, D., Malhi, Y., Affum-Baffoe, K., Castanho, A. D., Doughty, C. E., Fisher, R. A., Lewis, S. L., Peh, K. S.-H., Phillips, O. L., Quesada, C. A., et al.: Residence times of woody biomass in tropical forests, Plant Ecol. Divers., 6, 139–157, 605 https://doi.org/10.1080/17550874.2013.770578, 2013.

Gatti, L. V., Basso, L. S., Miller, J. B., Gloor, M., Gatti Domingues, L., Cassol, H. L. G., Tejada, G., Aragão, L. E. O. C., Nobre, C., Peters, W., Marani, L., Arai, E., Sanches, A. H., Corrêa, S. M., Anderson, L., Von Randow, C., Correia, C. S. C., Crispim, S. P., and Neves, R. A. L.: Amazonia as a carbon source linked to deforestation and climate change, Nature, 595, 388–393, https://doi.org/10.1038/s41586-021-03629-6, 2021.

610 Gaui, T. D., Costa, F. R. C., de Souza, F. C., Amaral, M. R. M., de Carvalho, D. C., Reis, F. Q., and Higuchi, N.: Long-term effect of selective logging on floristic composition: A 25 year experiment in the Brazilian Amazon, Forest Ecol. Manag., 440, 258–266, https://doi.org/10.1016/j.foreco.2019.02.033, 2019.

GBIF.org: GBIF Homepage, https://www.gbif.org/, last access: 2021-01-10, 2021.

Gora, E. M. and Esquivel-Muelbert, A.: Implications of size-dependent tree mortality for tropical forest carbon dynamics, Nat. Plants, 7, 615 384–391, https://doi.org/10.1038/s41477-021-00879-0, 2021.

Greenwood, S., Ruiz-Benito, P., Martínez-Vilalta, J., Lloret, F., Kitzberger, T., Allen, C. D., Fensham, R., Laughlin, D. C., Kattge, J., Bönisch, G., et al.: Tree mortality across biomes is promoted by drought intensity, lower wood density and higher specific leaf area, Ecol. Lett., 20, 539–553, https://doi.org/10.1111/ele.12748, 2017.

Harper, A. B., Cox, P. M., Friedlingstein, P., Wiltshire, A. J., Jones, C. D., Sitch, S., Mercado, L. M., Groenendijk, M., Robertson, E., Kattge, 620 J., et al.: Improved representation of plant functional types and physiology in the Joint UK Land Environment Simulator (JULES v4.2) using plant trait information, Geosci. Model Dev., 9, 2415–2440, https://doi.org/10.5194/gmd-9-2415-2016, 2016.

Harper, A. B., Wiltshire, A. J., Cox, P. M., Friedlingstein, P., Jones, C. D., Mercado, L. M., Sitch, S., Williams, K., and Duran-Rojas, C.: Vegetation distribution and terrestrial carbon cycle in a carbon cycle configuration of JULES4.6 with new plant functional types, Geosci. Model Dev., 11, 2857–2873, https://doi.org/10.5194/gmd-11-2857-2018, 2018.

625 Harris, N. L., Gibbs, D. A., Baccini, A., Birdsey, R. A., De Bruin, S., Farina, M., Fatoyinbo, L., Hansen, M. C., Herold, M., Houghton, R. A., et al.: Global maps of twenty-first century forest carbon fluxes, Nat. Clim. Change, 11, 234–240, https://doi.org/10.1038/s41558-020-00976-6, 2021.

Hu, T., Su, Y., Xue, B., Liu, J., Zhao, X., Fang, J., and Guo, Q.: Mapping global forest aboveground biomass with spaceborne LiDAR, optical imagery, and forest inventory data, Remote Sens., 8, 565, https://doi.org/10.3390/rs8070565, 2016.

630 Hubau, W., Lewis, S. L., Phillips, O. L., Affum-Baffoe, K., Beeckman, H., Cuní-Sanchez, A., Daniels, A. K., Ewango, C. E., Fauset, S., Mukinzi, J. M., et al.: Asynchronous carbon sink saturation in African and Amazonian tropical forests, Nature, 579, 80–87, https://doi.org/10.1038/s41586-020-2035-0, 2020.

Jiménez-Muñoz, J. C., Mattar, C., Barichivich, J., Santamaría-Artigas, A., Takahashi, K., Malhi, Y., Sobrino, J. A., and Van Der Schrier, G.: Record-breaking warming and extreme drought in the Amazon rainforest during the course of El Niño 2015–2016, Sci. Rep., 6, 1–7, 635 https://doi.org/10.1038/srep33130, 2016.

Johnson, M. O., Galbraith, D., Gloor, M., De Deurwaerder, H., Guimberteau, M., Rammig, A., Thonicke, K., Verbeeck, H., Von Randow, C., Monteagudo, A., et al.: Variation in stem mortality rates determines patterns of above-ground biomass in Amazonian forests: implications for dynamic global vegetation models, Glob. Change Biol., 22, 3996–4013, https://doi.org/10.1111/gcb.13315, 2016.

Keeling, H. C. and Phillips, O. L.: The global relationship between forest productivity and biomass, Global Ecol. Biogeogr., 16, 618–631, https://doi.org/10.1111/j.1466-8238.2007.00314.x, 2007.

King, D. A., Davies, S. J., Tan, S., and Noor, N. S. M.: The role of wood density and stem support costs in the growth and mortality of tropical trees, J. Ecol., 94, 670–680, https://doi.org/10.1111/j.1365-2745.2006.01112.x, 2006.

Kraft, N. J., Metz, M. R., Condit, R. S., and Chave, J.: The relationship between wood density and mortality in a global tropical forest data set, New Phytol., 188, 1124–1136, https://doi.org/10.1111/j.1469-8137.2010.03444.x, 2010.

Larjavaara, M. and Muller-Landau, H. C.: Rethinking the value of high wood density, Funct. Ecol., 24, 701–705, https://doi.org/10.1111/j.1365-2435.2010.01698.x, 2010.

Le Toan, T., Planells, M., Bouvet, A., Mermoz, S., Lucas, R., Ryan, C., Pathe, C., Dubois, C., Carreiras, J., Bowers, S., Kay, H., Bunting, P., Rodriguez-Veiga, P., and S., Q.: Product Validation and Algorithm Selection Report v2, https://climate.esa.int/sites/default/files/Biomass_D2.1_Porduvct_Validation_and_Algorithm_Selection_Report_V2.0.pdf, last access: 2022-20-03, 2020.

Liang, X., Ye, Q., Liu, H., and Brodribb, T. J.: Wood density predicts mortality threshold for diverse trees, New Phytol., 229, 3053–3057, https://doi.org/10.1111/nph.17117, 2021.

Lugo, A. E. and Scatena, F. N.: Background and catastrophic tree mortality in tropical moist, wet, and rain forests, Biotropica, 28, 585–599, https://doi.org/10.2307/2389099, 1996.

Magnabosco Marra, D., Trumbore, S. E., Higuchi, N., Ribeiro, G. H., Negrón-Juárez, R. I., Holzwarth, F., Rifai, S. W., Dos Santos, J., Lima, A. J., Kinupp, V. F., et al.: Windthrows control biomass patterns and functional composition of Amazon forests, Glob. Change Biol., 24, 5867–5881, https://doi.org/10.1111/gcb.14457, 2018.

Malhi, Y. and Wright, J.: Spatial patterns and recent trends in the climate of tropical rainforest regions, Philos. T. R. Soc. B, 359, 311–329, https://doi.org/10.1098/rstb.2003.1433, 2004.

Malhi, Y., Baker, T. R., Phillips, O. L., Almeida, S., Alvarez, E., Arroyo, L., Chave, J., Czimczik, C. I., Fiore, A. D., Higuchi, N., et al.: The above-ground coarse wood productivity of 104 Neotropical forest plots, Glob. Change Biol., 10, 563–591, https://doi.org/10.1111/j.1529-8817.2003.00778.x, 2004.

Malhi, Y., Wood, D., Baker, T. R., Wright, J., Phillips, O. L., Cochrane, T., Meir, P., Chave, J., Almeida, S., Arroyo, L., et al.: The regional variation of aboveground live biomass in old-growth Amazonian forests, Glob. Change Biol., 12, 1107–1138, https://doi.org/10.1111/j.1365-2486.2006.01120.x, 2006.

Malhi, Y., Doughty, C. E., Goldsmith, G. R., Metcalfe, D. B., Girardin, C. A., Marthews, T. R., del Aguila-Pasquel, J., Aragão, L. E., Araujo-Murakami, A., Brando, P., et al.: The linkages between photosynthesis, productivity, growth and biomass in lowland Amazonian forests, Glob. Change Biol., 21, 2283–2295, https://doi.org/10.1111/gcb.12859, 2015.

MapBiomas: Amazonia Project - Collection 2.0 of Amazonian Annual Land Cover and Land Use Map Series, http://amazonia.mapbiomas.org, last access: 2021-23-10, 2021.

Maréchaux, I. and Chave, J.: An individual-based forest model to jointly simulate carbon and tree diversity in Amazonia: description and applications, Ecol. Monogr., 87, 632–664, https://doi.org/10.1002/ecm.1271, 2017.

Maréchaux, I., Bartlett, M. K., Sack, L., Baraloto, C., Engel, J., Joetzjer, E., and Chave, J.: Drought tolerance as predicted by leaf water potential at turgor loss point varies strongly across species within an Amazonian forest, Funct. Ecol., 29, 1268–1277, https://doi.org/10.1111/1365-2435.12452, 2015.

675 Maréchaux, I., Langerwisch, F., Huth, A., Bugmann, H., Morin, X., Reyer, C. P., Seidl, R., Collalti, A., Dantas de Paula, M., Fischer, R., et al.: Tackling unresolved questions in forest ecology: The past and future role of simulation models, Ecol. Evol., 11, 3746–3770, https://doi.org/10.1002/ece3.7391, 2021.

McCulloh, K. A., Meinzer, F. C., Sperry, J. S., Lachenbruch, B., Voelker, S. L., Woodruff, D. R., and Domec, J.-C.: Comparative hydraulic architecture of tropical tree species representing a range of successional stages and wood density, Oecologia, 167, 27–37,
680 https://doi.org/10.1007/s00442-011-1973-5, 2011.

McDowell, N., Allen, C. D., Anderson-Teixeira, K., Brando, P., Brienen, R., Chambers, J., Christoffersen, B., Davies, S., Doughty, C., Duque, A., et al.: Drivers and mechanisms of tree mortality in moist tropical forests, New Phytol., 219, 851–869, https://doi.org/10.1111/nph.15027, 2018.

Mensah, S., Kakaï, R. G., and Seifert, T.: Patterns of biomass allocation between foliage and woody structure: the effects of tree size and
685 specific functional traits, Ann. For. Res., 59, 49–60, https://doi.org/10.15287/afr.2016.458, 2016.

Mercado, L. M., Patino, S., Domingues, T. F., Fyllas, N. M., Weedon, G. P., Sitch, S., Quesada, C. A., Phillips, O. L., Aragão, L. E., Malhi, Y., et al.: Variations in Amazon forest productivity correlated with foliar nutrients and modelled rates of photosynthetic carbon supply, Philos. T. R. Soc. B, 366, 3316–3329, https://doi.org/10.1098/rstb.2011.0045, 2011.

Mitchard, E. T., Feldpausch, T. R., Brienen, R. J., Lopez-Gonzalez, G., Monteagudo, A., Baker, T. R., Lewis, S. L., Lloyd, J., Quesada, C. A.,
690 Gloor, M., et al.: Markedly divergent estimates of Amazon forest carbon density from ground plots and satellites, Global Ecol. Biogeogr., 23, 935–946, https://doi.org/10.1111/geb.12168, 2014.

Moorcroft, P. R., Hurtt, G. C., and Pacala, S. W.: A method for scaling vegetation dynamics: the ecosystem demography model (ED), Ecol. Monogr., 71, 557–586, https://doi.org/10.1890/0012-9615(2001)071[0557:AMFSVD]2.0.CO;2, 2001.

Muller-Landau, H. C.: Interspecific and inter-site variation in wood specific gravity of tropical trees, Biotropica, 36, 20–32,
695 https://doi.org/10.1111/j.1744-7429.2004.tb00292.x, 2004.

Myers, N., Mittermeier, R. A., Mittermeier, C. G., Da Fonseca, G. A., and Kent, J.: Biodiversity hotspots for conservation priorities, Nature, 403, 853–858, https://doi.org/10.1038/35002501, 2000.

Nakhavali, M., Mercado, L. M., Hartley, I. P., Sitch, S., Cunha, F. V., di Ponzio, R., Lugli, L. F., Quesada, C. A., Andersen, K. M., Chadburn, S. E., et al.: Representation of phosphorus cycle in Joint UK Land Environment Simulator (vn5. 5_JULES-CNP), Geosci. Model Dev.
700 Discussions [preprint], pp. 1–24, https://doi.org/10.5194/gmd-2021-403, in review, 2021.

Nascimento, H. E., Laurance, W. F., Condit, R., Laurance, S. G., D'Angelo, S., and Andrade, A. C.: Demographic and life-history correlates for Amazonian trees, J. Veg. Sci., 16, 625–634, https://doi.org/10.1111/j.1654-1103.2005.tb02405.x, 2005.

Negrón-Juárez, R. I., Holm, J. A., Marra, D. M., Rifai, S. W., Riley, W. J., Chambers, J. Q., Koven, C. D., Knox, R. G., McGroddy, M. E., Di Vittorio, A. V., et al.: Vulnerability of Amazon forests to storm-driven tree mortality, Environ. Res. Lett., 13, 054 021,
705 https://doi.org/10.1088/1748-9326/aabe9f, 2018.

Nogueira, E. M., Nelson, B. W., Fearnside, P. M., França, M. B., and de Oliveira, Á. C. A.: Tree height in Brazil's 'arc of deforestation': shorter trees in south and southwest Amazonia imply lower biomass, Forest Ecol. Manag., 255, 2963–2972, https://doi.org/10.1016/j.foreco.2008.02.002, 2008.

Peacock, J., Baker, T., Lewis, S., Lopez-Gonzalez, G., and Phillips, O.: The RAINFOR database: monitoring forest biomass and dynamics,
710   J. Veg. Sci., 18, 535–542, https://doi.org/10.1111/j.1654-1103.2007.tb02568.x, 2007.

Phillips, O. L., Lewis, S. L., Baker, T. R., Chao, K.-J., and Higuchi, N.: The changing Amazon forest, Philos. T. R. Soc. B, 363, 1819–1827,
    https://doi.org/10.1098/rstb.2007.0033, 2008.

Ploton, P., Mortier, F., Réjou-Méchain, M., Barbier, N., Picard, N., Rossi, V., Dormann, C., Cornu, G., Viennois, G., Bayol, N.,
    et al.: Spatial validation reveals poor predictive performance of large-scale ecological mapping models, Nat. Commun., 11, 1–11,
715   https://doi.org/10.1038/s41467-020-18321-y, 2020.

Poorter, L., Wright, S. J., Paz, H., Ackerly, D. D., Condit, R., Ibarra-Manríquez, G., Harms, K. E., Licona, J., Martinez-Ramos, M., Mazer,
    S., et al.: Are functional traits good predictors of demographic rates? Evidence from five neotropical forests, Ecology, 89, 1908–1920,
    https://doi.org/10.1890/07-0207.1, 2008.

Pugh, T. A., Rademacher, T., Shafer, S. L., Steinkamp, J., Barichivich, J., Beckage, B., Haverd, V., Harper, A., Heinke, J., Nishina, K., et al.:
720   Understanding the uncertainty in global forest carbon turnover, Biogeosciences, 17, 3961–3989, https://doi.org/10.5194/bg-17-3961-2020,
    2020.

Quesada, C., Lloyd, J., Schwarz, M., Patiño, S., Baker, T., Czimczik, C., Fyllas, N., Martinelli, L., Nardoto, G., Schmerler, J., et al.:
    Variations in chemical and physical properties of Amazon forest soils in relation to their genesis, Biogeosciences, 7, 1515–1541,
    https://doi.org/10.5194/bg-7-1515-2010, 2010.

725 Quesada, C. A., Phillips, O. L., Schwarz, M., Czimczik, C. I., Baker, T. R., Patiño, S., Fyllas, N. M., Hodnett, M. G., Herrera, R., Almeida,
    S., et al.: Basin-wide variations in Amazon forest structure and function are mediated by both soils and climate, Biogeosciences, 9,
    2203–2246, https://doi.org/10.5194/bg-9-2203-2012, 2012.

Rödig, E., Cuntz, M., Heinke, J., Rammig, A., and Huth, A.: Spatial heterogeneity of biomass and forest structure of the Amazon rain forest:
    Linking remote sensing, forest modelling and field inventory, Global Ecol. Biogeogr., 26, 1292–1302, https://doi.org/10.1111/geb.12639,
730   2017.

Saatchi, S. S., Houghton, R. A., Dos Santos Alvala, R., Soares, J. V., and Yu, Y.: Distribution of aboveground live biomass in the Amazon
    basin, Glob. Change Biol., 13, 816–837, https://doi.org/10.1111/j.1365-2486.2007.01323.x, 2007.

Saatchi, S. S., Harris, N. L., Brown, S., Lefsky, M., Mitchard, E. T., Salas, W., Zutta, B. R., Buermann, W., Lewis, S. L., Hagen, S.,
    et al.: Benchmark map of forest carbon stocks in tropical regions across three continents, P. Natl. Acad. Sci. USA, 108, 9899–9904,
735   https://doi.org/10.1073/pnas.1019576108, 2011.

Sakschewski, B., von Bloh, W., Boit, A., Rammig, A., Kattge, J., Poorter, L., Peñuelas, J., and Thonicke, K.: Leaf and stem eco-
    nomics spectra drive diversity of functional plant traits in a dynamic global vegetation model, Glob. Change Biol., 21, 2711–2725,
    https://doi.org/10.1111/gcb.12870, 2015.

Santoro, M. and Cartus, O.: ESA Biomass Climate Change Initiative (Biomass_cci): Global datasets of forest above-ground biomass for the
740   years 2010, 2017 and 2018 v2., Centre for Environmental Data Analysis, https://doi.org/10.5285/84403d09cef3485883158f4df2989b0c,
    2021.

Sellar, A. A., Jones, C. G., Mulcahy, J. P., Tang, Y., Yool, A., Wiltshire, A., O'connor, F. M., Stringer, M., Hill, R., Palmieri,
    J., et al.: UKESM1: Description and evaluation of the UK Earth System Model, J. Adv. Model. Earth Sy., 11, 4513–4558,
    https://doi.org/10.1029/2019MS001739, 2019.

745 Siau, J. F.: Basic Wood-Moisture Relationships, in: Transport processes in wood, pp. 1–34, Springer, https://doi.org/10.1007/978-3-642-
    69213-0_1, 1984.

Sitch, S., Friedlingstein, P., Gruber, N., Jones, S. D., Murray-Tortarolo, G., Ahlström, A., Doney, S. C., Graven, H., Heinze, C., Huntingford, C., et al.: Recent trends and drivers of regional sources and sinks of carbon dioxide, Biogeosciences, 12, 653–679, https://doi.org/10.5194/bg-12-653-2015, 2015.

750 Steffen, W., Rockström, J., Richardson, K., Lenton, T. M., Folke, C., Liverman, D., Summerhayes, C. P., Barnosky, A. D., Cornell, S. E., Crucifix, M., et al.: Trajectories of the Earth System in the Anthropocene, P. Natl. Acad. Sci. USA, 115, 8252–8259, https://doi.org/10.1073/pnas.1810141115, 2018.

Sun, Y., Goll, D. S., Chang, J., Ciais, P., Guenet, B., Helfenstein, J., Huang, Y., Lauerwald, R., Maignan, F., Naipal, V., et al.: Global evaluation of the nutrient-enabled version of the land surface model ORCHIDEE-CNP v1.2 (r5986), Geosci. Model Dev., 14, 1987–2010, 755 https://doi.org/10.5194/gmd-14-1987-2021, 2021.

Swaine, M., Lieberman, D., and Putz, F. E.: The dynamics of tree populations in tropical forest: a review, J. Trop. Ecol., pp. 359–366, https://doi.org/10.1017/S0266467400002339, 1987.

Ter Steege, H., Pitman, N. C., Sabatier, D., Baraloto, C., Salomão, R. P., Guevara, J. E., Phillips, O. L., Castilho, C. V., Magnusson, W. E., Molino, J.-F., et al.: Hyperdominance in the Amazonian tree flora, Science, 342, 1243 092, https://doi.org/10.1126/science.1243092, 2013.

760 Ter Steege, H., Vaessen, R. W., Cárdenas-López, D., Sabatier, D., Antonelli, A., de Oliveira, S. M., Pitman, N. C., Jørgensen, P. M., and Salomão, R. P.: The discovery of the Amazonian tree flora with an updated checklist of all known tree taxa, Sci. Rep., 6, 1–15, https://doi.org/10.1038/srep29549, 2016.

Turner, D. P., Ritts, W. D., Cohen, W. B., Gower, S. T., Running, S. W., Zhao, M., Costa, M. H., Kirschbaum, A. A., Ham, J. M., Saleska, S. R., et al.: Evaluation of MODIS NPP and GPP products across multiple biomes, Remote Sens. Environ., 102, 282–292, 765 https://doi.org/10.1016/j.rse.2006.02.017, 2006.

Uhl, C. and Jordan, C. F.: Succession and nutrient dynamics following forest cutting and burning in Amazonia, Ecology, 65, 1476–1490, https://doi.org/10.2307/1939128, 1984.

Van Gelder, H., Poorter, L., and Sterck, F.: Wood mechanics, allometry, and life-history variation in a tropical rain forest tree community, New Phytol., 171, 367–378, https://doi.org/10.1111/j.1469-8137.2006.01757.x, 2006.

770 Vancutsem, C., Achard, F., Pekel, J.-F., Vieilledent, G., Carboni, S., Simonetti, D., Gallego, J., Aragao, L. E., and Nasi, R.: Long-term (1990–2019) monitoring of forest cover changes in the humid tropics, Science Advances, 7, eabe1603, https://doi.org/10.1126/sciadv.abe1603, 2021.

Wright, S. J., Kitajima, K., Kraft, N. J., Reich, P. B., Wright, I. J., Bunker, D. E., Condit, R., Dalling, J. W., Davies, S. J., Díaz, S., et al.: Functional traits and the growth–mortality trade-off in tropical trees, Ecology, 91, 3664–3674, https://doi.org/10.1890/09-2335.1, 2010.

775 Zanne, A. E., Lopez-Gonzalez, G., Coomes, D. A., Ilic, J., Jansen, S., Lewis, S. L., Miller, R. B., Swenson, N. G., Wiemann, M. C., and Chave, J.: Global wood density database, Dryad Digital Repository, http://hdl.handle.net/10255/dryad.235., 2009.

Zelinka, M. D., Myers, T. A., McCoy, D. T., Po-Chedley, S., Caldwell, P. M., Ceppi, P., Klein, S. A., and Taylor, K. E.: Causes of higher climate sensitivity in CMIP6 models, Geophys. Res. Lett., 47, e2019GL085 782, https://doi.org/10.1029/2019GL085782, 2020.

Zemp, D., Schleussner, C.-F., Barbosa, H., Van der Ent, R., Donges, J. F., Heinke, J., Sampaio, G., and Rammig, A.: On the importance 780 of cascading moisture recycling in South America, Atmos. Chem. Phys., 14, 13 337–13 359, https://doi.org/10.5194/acp-14-13337-2014, 2014.

Zhang, Y., Liang, S., and Yang, L.: A review of regional and global gridded forest biomass datasets, Remote Sens., 11, 2744, https://doi.org/10.3390/rs11232744, 2019.